



## Amphidomataceae (Dinophyceae) in the western Greenland area, including description of *Azadinium perforatum* sp. nov.

Urban Tillmann, Stephan Wietkamp, Bernd Krock, Anette Tillmann, Daniela Voss & Haifeng Gu

To cite this article: Urban Tillmann, Stephan Wietkamp, Bernd Krock, Anette Tillmann, Daniela Voss & Haifeng Gu (2020) Amphidomataceae (Dinophyceae) in the western Greenland area, including description of *Azadinium perforatum* sp. nov., *Phycologia*, 59:1, 63-88, DOI: [10.1080/00318884.2019.1670013](https://doi.org/10.1080/00318884.2019.1670013)


To link to this article: <https://doi.org/10.1080/00318884.2019.1670013>

 View supplementary material 

 Published online: 02 Dec 2019.

 Submit your article to this journal 

 Article views: 62

 View related articles 

 View Crossmark data 



## Amphidomataceae (Dinophyceae) in the western Greenland area, including description of *Azadinium perforatum* sp. nov.

URBAN TILLMANN<sup>1</sup>, STEPHAN WIETKAMP<sup>1</sup>, BERND KROCK<sup>1</sup>, ANETTE TILLMANN<sup>1</sup>, DANIELA VOSS<sup>2</sup>, AND HAIFENG GU <sup>3</sup>

<sup>1</sup>Alfred-Wegener-Institute, Helmholtz Centre for Polar and Marine Research, Am Handelshafen 12, Bremerhaven, D-27570, Germany

<sup>2</sup>Institute for Chemistry and Biology of the Marine Environment (ICBM), Carl von Ossietzky Universität Oldenburg, Schleusenstraße 1, Wilhelmshaven, D-26382, Germany

<sup>3</sup>Third Institute of Oceanography, Ministry of Natural Resources, Xiamen, 361005, China

### ABSTRACT

Azaspiracids (AZA) are lipophilic marine biotoxins associated with shellfish poisoning which are produced by some species of Amphidomataceae. Diversity and global biogeography of this family are still poorly known. In summer 2017 plankton samples were collected from the central Labrador Sea and western Greenland coast from 64° N (Gothaab Fjord) to 75° N for the presence of Amphidomataceae and AZA. In the central Labrador Sea, light microscopy revealed small *Azadinium*-like cells (9200 cells l<sup>-1</sup>). Clonal strains established from plankton samples and scanning electron microscopy of fixed plankton samples revealed at least eight species of Amphidomataceae: *Azadinium obesum*, *Az. trinitatum*, *Az. dexteroporum*, *Az. spinosum*, *Az. polongum*, *Amphidoma languida*, *Azadinium* spec., and a new species described here as *Azadinium perforatum* sp. nov. The new species differed from other *Azadinium* species by the presence of thecal pores on the pore plate. All samples, including cultured strains, filtered seawater samples, and solid phase adsorption toxin tracking (SPATT) samplers deployed during the expedition in a continuous water-sampling system (FerryBox), were negative for AZA. DNA samples and PCR assays were positive for Amphidomataceae from most stations, whereas species-specific assays for three toxigenic species were rarely positive (two stations for *Az. poporum*, one station for *Am. languida*). The results highlight the presence of Amphidomataceae in the area but the lack of toxins and low abundance of toxigenic species currently indicate a low risk of toxic Amphidomataceae blooms in Arctic coastal waters.

### ARTICLE HISTORY

Received 16 May 2019  
Accepted 17 September 2019  
Published online 02  
December 2019

### KEYWORDS

*Amphidoma*; Azaspiracids;  
New species; Subarctic

## INTRODUCTION


Biodiversity and biogeography research of high latitude phytoplankton have a long history, starting with the first exploratory expeditions in the mid-19th and early twentieth century (Brandt & Apstein 1908; Cleve 1873; Cleve & Grunow 1880; Ehrenberg 1843; Gran 1929; Grontved & Seidenfaden 1938; Lebour 1925). Extensive lists of plankton species from these survey reports are still the basis for contemporary taxonomic research in the Arctic. Such historical work and also more recent taxonomic studies are needed as an indispensable baseline in order to fully evaluate potential change in species diversity, and distribution and community composition in the area. This is of special importance for Arctic and subarctic areas, as significant and rapid temperature changes unprecedented in the observational record are occurring. Temperatures in the Arctic are increasing at a rate of two to three times the global average temperature in the past 150 years (Wassmann *et al.* 2011). Along with decreasing ice cover and increasing solar irradiance, temperature increases are expected to expand the spatial and temporal windows for survival, life cycle transitions and growth of a variety of plankton species, including those responsible for toxic, or harmful, algal blooms (HABs).

Current knowledge of Arctic plankton species diversity is biased towards large species collected and observed by classical plankton nets and light microscopy. Thus, species < 20 µm account for fewer than 20% of species in a more recent assessment of pan-Arctic biodiversity (Poulin *et al.* 2011). Recent biodiversity assessments of the area are based mainly on high throughput sequencing (Metfies *et al.* 2012; Elferink *et al.* 2017; Kiliyas *et al.* 2013, 2014; Wolf *et al.* 2015). While this approach reveals high diversity, especially in low size fractions (Elferink *et al.* 2017), high throughput sequencing still lacks species-level taxonomic resolution. However, species identification is especially necessary where closely related toxic and non-toxic species occur. Moreover, molecular diversity estimates always reveal a high degree of molecular signatures which cannot be linked to defined morphospecies (Medinger *et al.* 2010; Xiao *et al.* 2014), and this underlines the continuous and even increasing need for alpha taxonomy.

*Azadinium* and *Amphidoma* are the only genera of Amphidomataceae. They are good examples of small-sized nanoplankton described in the last decade, whose distribution and species diversity are not yet fully explored. This dinophycean family is of particular interest because some species produce

**CONTACT** Urban Tillmann  [urban.tillmann@awi.de](mailto:urban.tillmann@awi.de)

Colour versions of one or more of the figures in the article can be found online at [www.tandfonline.com/uphy](http://www.tandfonline.com/uphy).

 Supplemental data for this article can be accessed on the [publisher's website](http://publisher's website).

azaspiracids (AZA), a group of lipophilic compounds which accumulate in shellfish (Hess *et al.* 2014; Twiner *et al.* 2014). The presence of AZA in field plankton samples and/or shellfish in Arctic and subarctic areas has not yet been reported, but that might reflect a lack of targeted studies. In any case, there is evidence for the presence of Amphidomataceae in cold northern waters. The non-toxigenic *Azadinium caudatum* (Halldal) Nézan & Chomérat was described from the northern Norwegian coast in winter (Halldal 1953) and is common, and at times numerous, along the Norwegian coast (Thronsdén *et al.* 2007). A dinophyte described as *Gonyaulax parva* Ramsfjell from the central Norwegian Sea towards Iceland (Ramsfjell 1959) is almost certainly a species of *Azadinium* (see discussion in Tillmann *et al.* 2014a); furthermore, other species from the Canadian Arctic (Bérard-Therriault *et al.* 1999; Holmes 1956), labelled as '*Gonyaulax gracilis*' (which was depicted and invalidly described by J. Schiller in 1935), probably refers to a species of *Azadinium* (see discussion in Tillmann *et al.* 2014a). Finally, three new, but non-toxigenic, species of *Azadinium*, *Az. trinitatum* Tillmann & Nézan, *Az. cuneatum* Tillmann & Nézan, and *Az. concinnum* Tillmann & Nézan, were recently described from the North Atlantic Ocean around Iceland and the Irminger Sea (Tillmann *et al.* 2014a). In addition, toxigenic *Amphidoma languida* Tillmann, Salas & Elbrächter (producing AZA-38 and -39) and non-toxigenic *Az. dexteroporum* Percopo & Zingone were isolated from the area as well (Tillmann *et al.* 2015). Presence, diversity and distribution of Amphidomataceae on the western Greenland coast are currently unknown. A main reason for a lack of records and distribution data is that many species of Amphidomataceae are small (<20 µm cell length) and inconspicuous, and thus often go unnoticed in routine light microscopy. Amphidomataceae are thus a good example of the necessity of applying specific molecular detection tools. A family-specific molecular PCR assay detecting all Amphidomataceae (Smith *et al.* 2016) and species-specific qPCR assays for three of the toxigenic species (Toebe *et al.* 2013; Wietkamp *et al.* 2019a) are both available. From a chemical perspective, detection of AZA using LC-MS/MS can be a complementary and sensitive analytical tool for records of toxigenic Amphidomataceae, especially when long-term Solid Phase Adsorption Toxin Tracking (SPATT) deployments allow for integration and amplification of low signal levels.

On a research survey on the *RV Maria S. Merian* to the west coast of Greenland, we combined traditional onboard live microscopy with qPCR molecular detection and LC-MS/MS analysis (both discrete plankton samples and continuously deployed SPATT samplers) to specifically investigate the presence, diversity and distribution of amphidomatacean species. This baseline information evaluates the risk potential of azaspiric acid shellfish poisoning (AZP) in subarctic and Arctic waters.

## MATERIAL & METHODS

### Hydrographic observations and sampling

Data were collected from 25 June to 19 July 2017 onboard *RV Maria S. Merian* (MSM65) in the central Labrador Sea and along the western coast of Greenland (Fig. 1). At each station, CTD profiles were conducted using a Seabird 'sbe911+' CTD (Sea-Bird Electronics Inc., Seattle, Washington, USA) attached to

a sampling rosette. The CTD was equipped with a chlorophyll fluorescence sensor (Fluorometer, WET Labs, Philomath, Oregon, USA). Data acquisition was carried out via CTD-client on-board; post-processing was done with Seasoft V2. Temperature was corrected to ITS-90 (Preston-Thomas 1990). A total of 50 CTD stations (Fig. 1) from the central Labrador Sea and along the western coast of Greenland were sampled from specific depths using Niskin bottles. CTD Profiles are available at Pangaea (Zielinski *et al.* 2018). Data from surface waters (Fig. 2) represent the upper 5 m of each CTD cast. Graphics were generated using Ocean Data View (ODV) software (Schlitzer 2018).

Besides CTD casts at each station, surface water of the whole cruise track was investigated for temperature, salinity (model SBE45, Sea-Bird Electronics Inc., Seattle, Washington, USA) and fluorescence (model cyclops 7, Turner Design Inc., San Jose, California, USA) using a Pocket FerryBox (4H Jena, Jena, Germany). Data are available on request. The outlet of the FerryBox offers further options for sampling, e.g., for toxins.

### Sample processing

Niskin bottle samples from three depths (3 m, 10 m, and depth of the chlorophyll maximum) were fixed with Lugol's iodine (1% final concentration). For quantitative plankton counts, samples of these three depths were pooled, and 50 ml and 10 ml were settled in Utermöhl sedimentation chambers and counted with an IMR inverted microscope (Olympus, Hamburg, Germany). Counted subsample volume and magnification were adjusted for each species or protist group depending on the respective abundance. In addition, mixed water samples from three depths were used for on-board living plankton microscope observations. A 1-l sample was pre-screened (20 µm Nitex mesh) and gently concentrated by gravity filtration using a 5-µm polycarbonate filter (47-mm diameter, Millipore, Eschborn, Germany). A subsample was fixed with formaldehyde (1% final concentration) for later SEM analysis, and the rest was examined using an inverted microscope (Axiovert 200M, Zeiss, Göttingen, Germany). Samples were screened for cells of *Azadinium* and *Amphidoma* at high magnification (x640) based on general cell size and shape, on the presence of a theca, and on the presence of a distinctly pointed apex. Cells of interest were photographed with a digital camera (AxioCam MRc5, Zeiss).

### DNA extraction and PCR analysis

Plankton samples were collected at each station with Niskin bottles from 3 m, 10 m and from the chlorophyll maximum layer. Three litres of seawater from each depth were pre-screened through a 20-µm mesh Nitex sieve, and subsequently pooled. An amount of 3–5 l (depending on particle content) was filtered under gentle vacuum (< 200 mbar) through 5-µm pore-size polycarbonate filters (47-mm diameter, Millipore). Filters were attached to the inner wall of a 50-ml plastic centrifuge tube, and repeatedly rinsed with 1 ml pre-heated (60 °C) DNA lysis buffer (PL 1 buffer of the NucleoSpin Plant II kit, Macherey & Nagel, Düren, Germany). The lysis buffer was subsequently transferred into a 5-ml cryovial prefilled with 200-mg glass beads (acid-washed, grain size 212–300 µm, Sigma Aldrich, St. Louis, Missouri, USA) and stored at –20 °C. Not later than 1 week

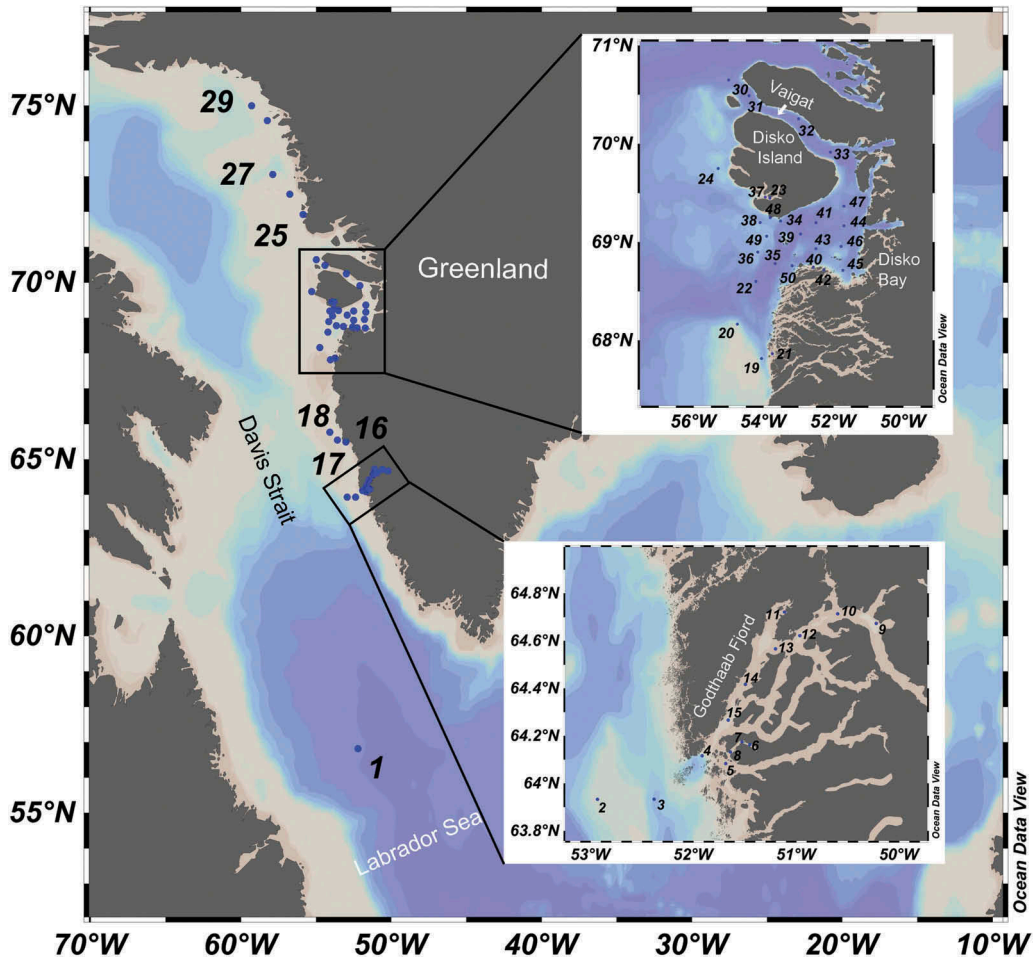


**Fig. 1.** Map of investigated area and location of stations of RV *Maria S. Merian* MSM65 cruise, 2017. Range in colours corresponds to different contour lines of water depth.

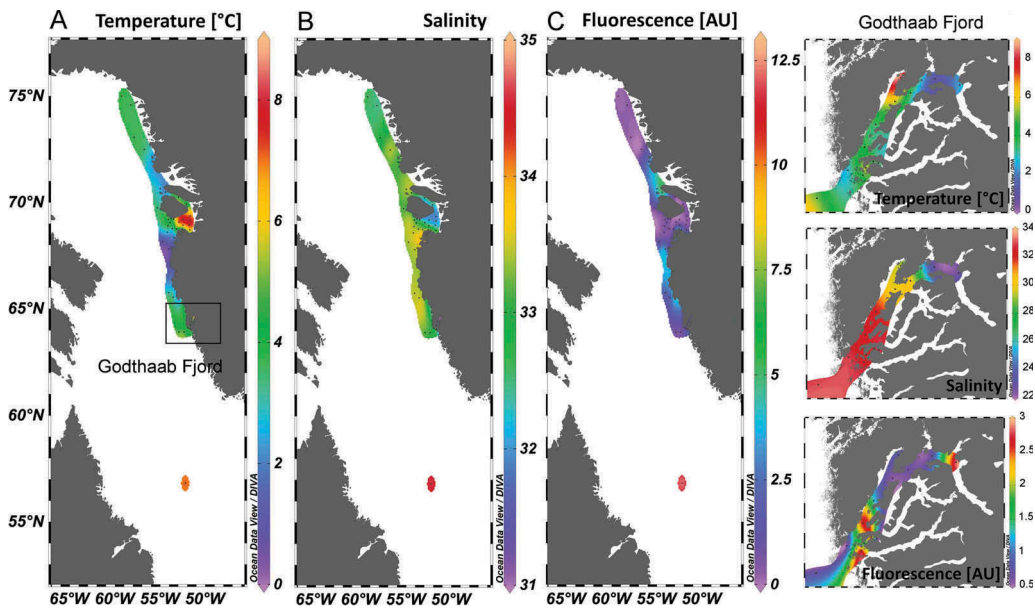


**Fig. 2.** Temperature (A), salinity (B) and fluorescence (C) in surface waters over the whole transect of the MSM65 campaign. The right panel shows cut-outs of the Godthaab Fjord area.



after sampling, DNA was extracted using the NucleoSpin Plant II kit (Macherey & Nagel) according to manufacturer's instructions.

SYBR Green PCR assays with family-specific amphidomatacean primers introduced by Smith *et al.* (2016) were performed on DNA extracts as a molecular pre-scanning method. One reaction contained 5  $\mu\text{l}$  of Fast SYBR Green Master Mix (Applied Biosystems by Thermo Fisher Scientific, Waltham, Massachusetts, USA), 3.5  $\mu\text{l}$  of high-grade PCR  $\text{H}_2\text{O}$ , 0.25  $\mu\text{l}$  of both primers (each 10  $\mu\text{M}$ , at a final concentration of 200 nM) and 1  $\mu\text{l}$  of template DNA. Plates were analysed on a StepOne Plus real-time PCR cycler (Applied Biosystems by Thermo Fisher Scientific) following these steps: initial preheating to 95 °C for 20 s, 40 cycles of 3 s at 95 °C and 30 s at 60 °C. The subsequent melt curve was performed for 15 s at 95 °C, 60 s at 60 °C and 15 s at 95 °C. Positive controls with known DNA concentrations as well as no-template controls (NTC) containing high-grade, nuclease-free water, were present in all PCR reactions. Primer performance and reactions were evaluated in terms of specificity and sensitivity. Melt-curve analysis was done for every reaction. Samples were analysed in triplicate, and were considered positive if at least two of the three replicates showed a fluorescence signal above the threshold before cycle 37.

Samples which showed positive results in the SYBR Green assay were tested with specific TaqMan qPCR assays on *Az. spinosum*, *Az. poporum* and *Am. languida* as described in Toebe *et al.* (2013) and Wietkamp *et al.* (2019a). Measurements were performed in triplicate. Each run contained non-template controls (NTC) and positive controls. Quantitative analyses were based on DNA standard curves as tenfold dilution series of target species' DNA (10 ng  $\mu\text{l}^{-1}$  to 10 fg  $\mu\text{l}^{-1}$ ) from cultures of *Az. spinosum* (3D9), *Az. poporum* (UTH-D4) and *Am. languida* (Z-LF-9-C9). For the limits of detection (LOD) and of quantification (LOQ), the definitions of Forootan *et al.* (2017) were applied. However, for standard curves of all three qPCR assays, the limited resolution of dilutions applied here did not allow differentiating between LOD and LOQ, which was 0.1 pg  $\mu\text{l}^{-1}$  sample extract.

### Azaspiracids

For AZA analysis of field plankton samples from discrete depths, samples were prepared and filtered as described above. Filters were placed with their back to the inner wall of a 50-ml centrifuge tube (Sarstedt, Nümbrecht, Germany), and were repeatedly rinsed with 500–1000  $\mu\text{l}$  methanol until complete decolouration of the filters. The methanolic extracts were transferred to a spin-filter (Ultrafree, 0.45- $\mu\text{m}$  pore-size, Millipore, Eschborn, Germany), centrifuged for 30 s at 800 x g, followed by transfer into autosampler vials and stored at –20 °C until measurement.

Additional samples were taken using a FerryBox continuous sampling system. Solid Phase Adsorption Toxin Tracking (SPATT) bags (100- $\mu\text{m}$  mesh, 10 g HP-20) were placed in a 7.5-l plastic container that was fed by the outflow of a FerryBox system at a flow rate of *c.* 2 litres  $\text{min}^{-1}$ , which in turn was supplied by the ship seawater system. During the entire expedition, three SPATT bags were deployed: SP1: 26 June (station 2) – 04 July (station 16), Labrador Sea – Godthaab Fjord (Nuup Kargerlua); SP2: 04 July (station 16) – 11 July (station 31),

Maniitsoq transect north – Vaigat (Sullorsuaq Strait); and SP3: 11 July (station 31) – 17 July (station 50), Vaigat – Disko Bay (Qeqertarsuup tunua).

Mass spectral experiments were performed to survey a wide array of AZA with an analytical system consisting of triple quadrupole mass spectrometer (API 4000 QTrap, Sciex, Darmstadt, Germany) equipped with a TurboSpray interface coupled to LC equipment (model LC 1100, Agilent, Waldbronn, Germany) that included a solvent reservoir, in-line degasser (G1379A), binary pump (G1311A), refrigerated autosampler (G1329A/G1330B), and temperature-controlled column oven (G1316A). Separation of AZA (5- $\mu\text{l}$  sample injection volume) was performed by reverse-phase chromatography on a C8 phase. The analytical column (50  $\times$  2 mm) was packed with 3  $\mu\text{m}$  Hypersil BDS 120 Å (Phenomenex, Aschaffenburg, Germany) and maintained at 20 °C. The flow rate was 0.2 ml  $\text{min}^{-1}$ , and gradient elution was performed with two eluents, where eluent A was water and eluent B was acetonitrile/water (95:5 v/v), both containing 2.0 mM ammonium formate and 50 mM formic acid. Initial conditions were 8-min column equilibration with 30% B, followed by a linear gradient to 100% B in 8 min and isocratic elution until 18 min with 100% B then returning to initial conditions until 21 min (total run time: 29 min). AZA profiles were determined in the selected reaction monitoring (SRM) mode in one period (0–18) min with curtain gas: 10 psi, CAD: medium, ion spray voltage: 5500 V, temperature: ambient, nebuliser gas: 10 psi, auxiliary gas: off, interface heater: on, declustering potential: 100 V, entrance potential: 10 V, exit potential: 30 V. SRM experiments were carried out in positive-ion mode by selecting the transitions shown in Table S1.

### On-board isolation and culture

On the first station in the central Labrador Sea, cells of Amphidomataceae were detected during the on-board live sample observations and were subsequently isolated using micro-capillaries into wells of 96-well plates filled with 0.2 ml filtered seawater. Cells were subsequently re-isolated a few times using a SZH-ILLD stereomicroscope (Olympus) equipped with dark field illumination into new wells of a 96-well plate. Plates were incubated at 10 °C under a photon flux density of *c.* 50  $\mu\text{mol m}^{-2} \text{s}^{-1}$  in a 16:8 h light:dark photoperiod in a controlled environment growth chamber (Model MIR 252, Sanyo Biomedical, Wood Dale, Illinois, USA).

### Characterisation of Amphidomataceae strains

After 4 weeks of growth, primary isolation plates from the cruise were inspected in the laboratory using a SZH-ILLD stereomicroscope (Olympus) for presence of *Azadinium*/*Amphidoma*-like cells as inferred from typical size, shape, and swimming behaviour. From each well with amphidomatacean cells, a clonal strain was established by isolation of single cells by micro-capillary. Established cultures were thus clonal but not axenic, and were routinely held in 70-ml plastic culture flasks at 15 °C in a natural seawater medium prepared with sterile filtered (0.2  $\mu\text{m}$  VacuCap filters, Pall Life Sciences, Dreieich, Germany) Antarctic seawater (salinity, 34; pH adjusted to 8.0), and enriched with 1/10 strength K-medium

(Keller *et al.* 1987) which was slightly modified by omitting ammonium ions.

For toxin analysis, strains were grown at 15 °C under a photon flux density of 50  $\mu\text{mol m}^{-2} \text{s}^{-1}$  on a 16:8 h light:dark photoperiod. For each harvest, cell density was determined by settling Lugol-fixed samples and counting > 800 cells using an inverted microscope. Densely grown strains (ranging from 0.5–5  $\times 10^4$  cells  $\text{ml}^{-1}$ ) were harvested by centrifugation (5810R, Eppendorf, Hamburg, Germany) of 50-ml subsamples at 3220  $\times g$  for 10 min. The cell pellet was resuspended, transferred into a microtube, centrifuged again (5415, Eppendorf, 16,000  $\times g$ , 5 min), and stored frozen (–20 °C) until use. For selected strains, growth and harvest procedures were repeated several times to yield a high biomass and consequently lower the cell quota-based limit of detection. Numbers of cells harvested for these strains are listed in Table S2. Several cell harvests of each strain were combined in 100  $\mu\text{l}$  of acetone. Extraction of cell pellets was repeated four times with 100  $\mu\text{l}$  each and combined cell suspensions were vortexed every 10 min for 1 h at room temperature. Homogenates were centrifuged (5810 R, Eppendorf) at 15 °C and 3220  $\times g$  for 15 min. Filtrates were then adjusted with acetone to a final volume of 0.5 ml. The extracts were transferred to a 0.45- $\mu\text{m}$  pore-size spin-filter (Millipore) and centrifuged (5415R, Eppendorf) at 800  $\times g$  for 30 s, with the resulting filtrate being transferred into a liquid chromatography (LC) autosampler vial for LC-MS/MS analysis.

For DNA extraction, each strain was grown in 70-ml plastic culture flasks under the standard culture conditions described above. Aliquots of 50 ml of healthy and growing culture (based on stereomicroscopic inspection of the live culture) were harvested by centrifugation (5819R, Eppendorf, 3000  $\times g$ , 10 min). Each pellet was transferred into a microtube, again centrifuged (5415, Eppendorf, 16,000  $\times g$ , 5 min), and stored at –80 °C until DNA extraction.

## MICROSCOPY

Observation of living and fixed cells was carried out with a SZH-ILLD stereomicroscope (Olympus) and an Axiovert 200 M inverted microscope (Zeiss). Observation and documentation of live cells at x1000 magnification were performed using an Axioskop 2 (Zeiss) and by recording videos using a Gryphax digital camera (Jenoptik, Jena, Germany) at full-HD resolution. Single frame micrographs were extracted using Corel VideoStudio software (Version X8 Pro). Photographs of formaldehyde-fixed cells (1% final concentration) were taken with an Axiocam MRc5 digital camera (Zeiss).

Cell length and width were measured at x1000 magnification using Axiovision software (Zeiss) and freshly fixed cells (formaldehyde, final concentration 1%) of strains growing at 15 °C.

For scanning electron microscopy (SEM), cells were collected by centrifugation (5810R, Eppendorf, 3220  $\times g$ , 10 min) of 15 ml of culture. The supernatant was removed and the cell pellet resuspended in 60% ethanol in a 2-ml microtube for 1 h, at 4 °C to strip off the outer cell membrane. Subsequently, cells were pelleted by centrifugation (5415R, Eppendorf, 16,000  $\times g$ , 5 min) and resuspended in a 60:40 mixture of deionised water and seawater for 30 min at 4 °C. After centrifugation and removal of the

diluted seawater supernatant, cells were fixed with formaldehyde (2% final concentration in a 60:40 mixture of deionised water and seawater) and stored at 4 °C for 3 h. Cells were then collected on polycarbonate filters (Millipore, 25-mm diameter, 3- $\mu\text{m}$  pore-size) in a filter funnel where all subsequent washing and dehydration steps were carried out. Eight washings (2-ml MilliQ-deionised water each) were followed by a dehydration series in ethanol (30%, 50%, 70%, 80%, 95%, 100%; 10 min each). Filters were dehydrated with hexamethyldisilazane (HMDS), first in 1:1 HMDS:EtOH, followed by twice in 100% HMDS, and then stored under gentle vacuum in a desiccator. Finally, filters were mounted on stubs, sputter coated (SC500, Emscope, Ashford, UK) with gold-palladium and viewed with a Quanta FEG 200 scanning electron microscope (FEI, Eindhoven, Netherlands). Some SEM micrographs were presented on a black background using Adobe Photoshop 6.0 (Adobe Systems, San Jose, California, USA). Labelling of dinophyte thecal plates was done according to the Kofoidian system.

## Molecular phylogeny

DNA extraction was performed using the NucleoSpin Plant II kit (Macherey & Nagel) according to manufacturer's instructions. Sequencing reactions of the 18S/small subunit (SSU), the Internal Transcribed Spacer region (ITS1, 5.8S rRNA, ITS2) and the D1/D2 region of 28S/large subunit (LSU) were performed as follows: polymerase chain reaction (PCR) was performed to amplify the aforementioned regions from the DNA extracts. Each reaction contained 16.3  $\mu\text{l}$  ultra-pure  $\text{H}_2\text{O}$ , 2.0  $\mu\text{l}$  HotMasterTaq buffer (5Prime, Hamburg, Germany), 0.2  $\mu\text{l}$  dNTPs (10  $\mu\text{M}$ ), 0.2  $\mu\text{l}$  of each primer (10  $\mu\text{M}$ ), 0.1  $\mu\text{l}$  of Taq Polymerase (Quantabio, Beverly, Massachusetts, USA) and 1.0  $\mu\text{l}$  of extracted DNA template (10 ng  $\mu\text{l}^{-1}$ ) to a final reaction volume of 20  $\mu\text{l}$ . PCR conditions for the amplification of the LSU and ITS were set as described in Wietkamp *et al.* (2019b) using the following primer sets: DirF (5'-ACC CGC TGA ATT TAA GCA TA-3') and D2CR (5'-CCT TGG TCC GTG TTT CAA GA-3') for LSU; ITSa (5'-CCA AGC TTC TAG ATC GTA ACA AGG (ACT)TC CGT AGG T-3') and ITSb (5'-CCT GCA GTC GAC A(GT)A TGC TTA A(AG)T TCA GC(AG) GG-3') for ITS. For SSU amplifications, the following settings were used: initialisation at 94 °C for 5 min; 30 cycles of 94 °C for 2 min, 55 °C for 2 min, 68 °C for 3 min; a final extension at 68 °C for 10 min. Forward and reverse primers for SSU amplification were: 1F (5' – AAC CTG GTT GAT CCT GCC AGT – 3') and 1528R (5' – TGA TCC TTC TGC AGG TTC ACC TAC – 3').

## Phylogenetic analysis

Newly obtained SSU, ITS and/or partial LSU rDNA sequences were incorporated into available *Amphidoma*, *Azadinium* and closely-related sequences in GenBank (<https://www.ncbi.nlm.nih.gov/genbank/>). Genbank accession numbers are listed in Table S3. Concatenated sequences were aligned using MAFFT v7.110 (Katoh & Standley 2013) online program (<http://mafft.cbrc.jp/alignment/server/>). Alignments were manually checked with BioEdit v7.0.5 (Hall 1999). For Bayesian inference (BI), jModelTest (Posada 2008) was used to select the most

appropriate model of molecular evolution using Akaike Information Criterion (AIC). Bayesian reconstruction of the data matrix was performed using MrBayes 3.2 (Ronquist & Huelsenbeck 2003) with the best-fitting substitution model (GTR+G). Four Markov chain Monte Carlo (MCMC) chains were run for 4,000,000 generations, sampling every 100 generations. Convergence diagnostics were estimated graphically using 'are we there yet?' (<http://ceb.scs.fsu.edu/awty>; Nylander *et al.* 2008), and the first 10% of burn-in trees were discarded. A majority-rule consensus tree was created to examine posterior probabilities of each clade. Maximum-likelihood (ML) analyses were conducted with RaxML v7.2.6 (Stamatakis 2006) on the T-REX web server (Boc *et al.* 2012) using the model GTR+G. Node support was assessed with 1000 bootstrap replicates.

Multiple ITS rDNA sequences of selected new strains were aligned with available *Amphidoma* and *Azadinium* sequences in GenBank using MAFFT v7.110 (Katoh & Standley 2013) online program with default settings. Completed alignments were imported into PAUP\* v4b10 (Swofford 2002) to estimate divergence rates using simple uncorrected pairwise (p) distance matrices.

### Chemical analysis of azaspiracids

Extracts of strains were screened for known AZA in the SRM mode as described above. In addition, precursor ion experiments were performed. Precursors of the characteristic AZA fragments  $m/z$  348,  $m/z$  360 and  $m/z$  362 were scanned in the positive-ion mode from  $m/z$  400 to 900 under the following conditions: curtain gas, 10 psi; CAD, medium; ion spray voltage, 5500 V; temperature, ambient; nebuliser gas, 10 psi; auxiliary gas, off; interface heater, on; declustering potential, 100 V; entrance potential, 10 V; collision energy, 70 V; exit potential, 12 V. Product ion spectra of the  $m/z$  values 830, 842 and 858 were recorded in the Enhanced Product Ion (EPI) mode in the mass range from  $m/z$  150 to 930. Positive ionisation and unit resolution mode were used. The following parameters were applied: curtain gas: 10 psi, CAD: medium, ion spray voltage: 5500 V, temperature: ambient, nebulizer gas: 10 psi, auxiliary gas: off, interface heater: on, declustering potential: 100 V, collision energy spread: 0, 10 V, collision energy: 70 V, exit potential, 12 V.

## RESULTS

### Hydrography

Surface temperature values ranged from *c.* 0.6 °C to 8.5 °C (Fig. 2). Highest surface temperatures were found in the Labrador Sea (Station 1) and the Disco Bay area, whereas the coastline had lower temperature (0.6 °C to 4.5 °C). Salinity values ranged from *c.* 22 to 35, with the lowest salinities found in the inner fjord section of Godthaab Fjord (*c.* 22) and Disco Bay, close to Jacobshaven (Illusiat; *c.* 31; Fig. 2). High fluorescence signals were identified in the Labrador Sea (*c.* 12 AU), at the entrance of the Vaigat area (4–5 AU), and within outer and inner section of the Godthaab Fjord (*c.* 3 AU; Fig. 2).

### General plankton composition

Phytoplankton composition and abundance determined from net tows and quantitative Uthermöhl counts revealed a high diversity of microplankton and locally quite different communities. This reflected late spring bloom dominance by diatoms, and/or high biomass of colonial flagellates such as *Phaeocystis pouchetii* (Harriot) Lagerheim and/or *Dinobryon balticum* (Schütt) Lemmermann, or post-bloom communities dominated by low densities of various dinoflagellate species. The first station in the open Labrador Sea revealed a high biomass of micro- and nanoplankton with noticeably high abundance of a small species of *Prorocentrum* and of an unknown haptophyte species. Along the Greenland coast and inside Godthaab Fjord and Disko Bay, plankton communities had high abundance of different species of flagellates and diatoms. Among the latter, there was a conspicuous bloom of *Chaetoceros debilis* Cleve in certain parts of the Godthaab Fjord, and locally high abundance of *Thalassiosira* spp. or *Chaetoceros socialis* H.S. Lauder in other parts of the study area. The most important and abundant flagellate species were two colony-forming species: the haptophyte *Phaeocystis pouchetii* and the chrysophyte *Dinobryon balticum*. Dinoflagellate communities consisted mainly of a highly diverse community of heterotrophic species (e.g., *Gyrodinium* spp., *Protoperidinium* spp., *Amphidinium* spp.) or undetermined species of unknown trophic status, whereas photosynthetic dinoflagellates (e.g., *Protoceratium reticulatum* (Claparède & Lachmann) Bütschli, *Dinophysis* spp., *Alexandrium* spp., *Margalefidinium* sp., *Heterocapsa* spp.) were generally of low abundance and biomass.

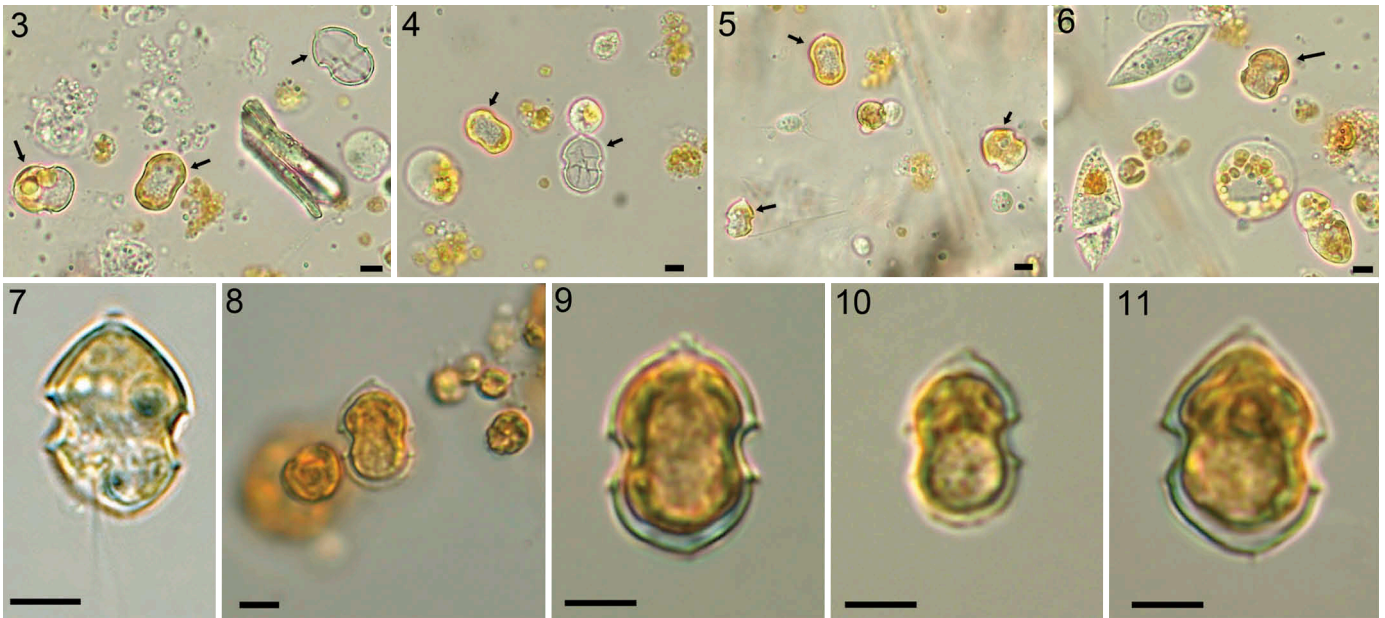
### On-board microscopy records of Amphidomataceae

On-board microscopy using live samples revealed the presence of Amphidomataceae at the first station in the central Labrador Sea (Figs 3–11). Identification was based on size, shape, and the presence of a distinctly pointed apex. No attempt was made to identify cells to species. Quantitative plankton counts using the sedimentation technique and Lugol-fixed samples revealed abundant, small, thecate dinoflagellates classified as *Azadinium/Amphidoma* (Figs 8–11) of 9200 cells ml<sup>-1</sup>. For all other stations inspected along the Greenland coast, no microscopic records of Amphidomataceae were noted with certainty.

### PCR assays

Of the 50 stations sampled, 33 were positive with the SYBR Green amphidomatacean PCR assay (Fig. 12). In Godthaab Fjord, negative hits were restricted to a few inner stations. Whereas most of the transit stations off the coast (stations 16–21, 25–27) were negative, Amphidomataceae were present at the two northernmost stations, and at all but four stations in the Disko Bay area. Positive hits of the species-specific qPCR assays were much more restricted. Considering the DNA extraction volume and the filtered water volume, the limit of detection of 0.1 pg target DNA µl<sup>-1</sup> corresponded here to *c.* 0.4–0.6 cells l<sup>-1</sup>.





**Figs 3–11.** Records of Amphidomataceae from the central Labrador Sea (station 1).

**Figs 3–7.** Living samples with amphidomatacean cells or empty thecae (both designated by arrows). Scale bars = 5  $\mu\text{m}$ .

**Figs 8–11.** Amphidomatacean cells in Lugol-fixed Utermöhl samples. Scale bars = 5  $\mu\text{m}$ .

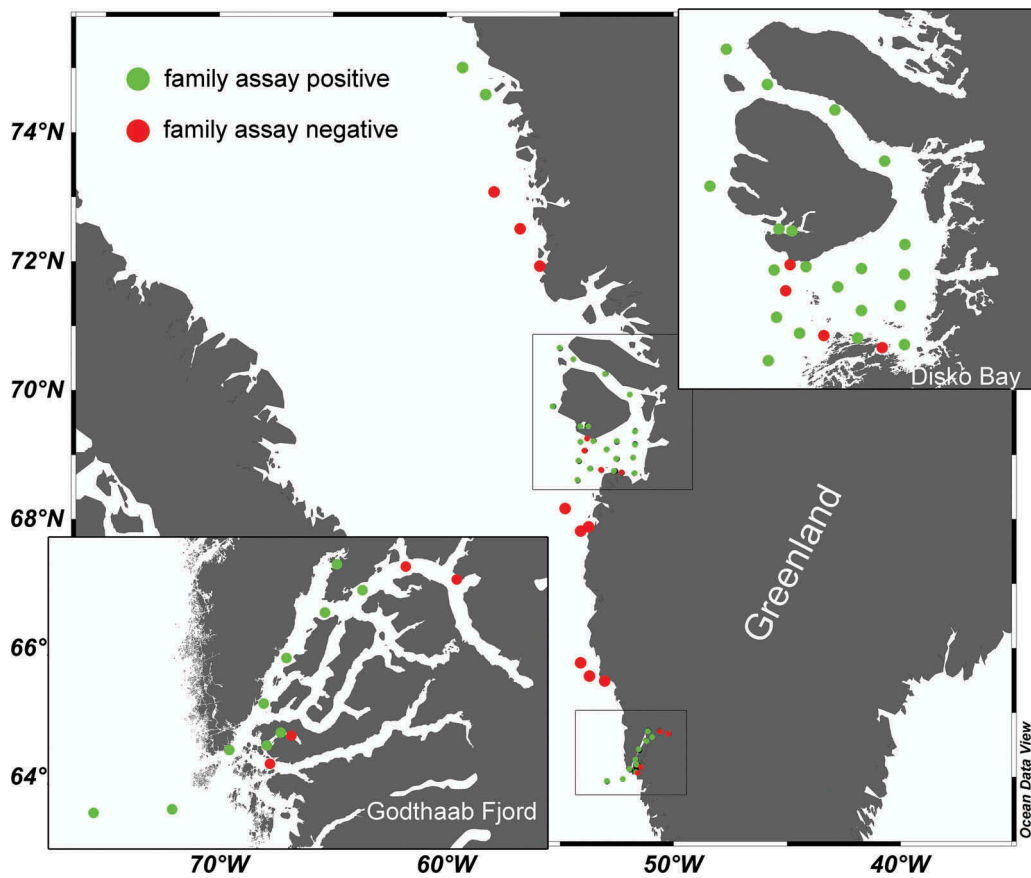


**Fig. 12.** Map showing PCR presence (green) or absence (red) of positive signals using Amphidomataceae family primers.

All samples were negative for *Az. spinosum* Elbrächter & Tillmann. *Amphidoma languida* was detected only at the first station in the central Labrador Sea with 117 cells  $\text{l}^{-1}$ . Positive

records with background abundance (1–2 cells  $\text{l}^{-1}$ ) for *Az. poporum* Tillmann & Elbrächter occurred at stations 14 and 22 only.



## AZA in field samples

None of the known AZA listed in Table S1 was detected in the 5–20 µm size fractions of seawater samples. The limits of detection (signal-to-noise ratio = 3) of these measurements ranged between 7 and 12 pg l<sup>-1</sup> seawater depending on water volume filtered and filter extraction volume. In addition to plankton samples, solid phase adsorption toxin tracking (SPATT) bags were continuously employed in a FerryBox sampling surface water throughout the expedition, but did not contain AZA above the LOD of 6 pg g<sup>-1</sup> resin.

## Azadinium, new strains

On-board single-cell isolation yielded 18 clonal amphidoma-tacean strains. All strains displayed a similar and conspicuous swimming behaviour consisting of a slow movement interrupted by short ‘jumps’ in various directions. Identification of all strains was based on morphology as examined by LM and SEM and was confirmed for all strains by rRNA sequence comparison (Table 1). The newly available strains comprised four species including *Az. obesum* Tillmann & Elbrächter (12 strains), *Az. trinitatum* (two strains), *Az. dexteroporum* (one strain), and three strains of a new species.

### *Azadinium perforatum* Tillmann, Wietkamp & H.Gu sp. nov. Figs 13–41

DESCRIPTION: Small photosynthetic thecate Dinophyceae; cells 14.6 to 20.0 µm long and 9.9 to 14.4 µm wide; cingulum broad (c. 20% of cell length) and postmedian; epitheca conical and ending in a small but distinctly pointed apical pore; hypotheca hemispherical with a very broad and long sulcus and with a single, very small antapical spine; tabulation formula: Po, cp, X, 6', 0a, 6'', 6C, 5S, 6''', 2'''; thecal pores present on the pore plate; a ventral pore located on the right ventral side in a notch of the pore plate.

HOLOTYPE: SEM stub prepared from clonal strain AZA-2H (designated CEDiT2019H103), deposited at the Senckenberg Research Institute and Natural History Museum, Centre of Excellence for Dinophyte Taxonomy (Wilhelmshaven, Germany).

ISOTYPES: Formalin-fixed sample prepared from clonal strain AZA-2H (designated CEDiT2019I104) deposited at the Senckenberg Research Institute and Natural History Museum, Centre of Excellence for Dinophyte Taxonomy (Wilhelmshaven, Germany)

TYPE LOCALITY: Central Labrador Sea (56°49.42'N; 52°13.15'W).

HABITAT: Marine plankton.

STRAIN ESTABLISHMENT: Sampled and isolated by U. Tillmann on 28 June 2017.

ETYMOLOGY: The epithet (Latin *perforatus* – pierced, penetrated) is inspired by the presence of small pores on the pore plate.

## Morphology

Using light and electron microscopy, all three clonal strains identified as *Az. perforatum* sp. nov. (AZA-2C, AZA-2E, AZA-2H) were identical in terms of morphology and plate pattern. The selected strain AZA-2H is described in detail.

Cells of *Az. perforatum* sp. nov. were ovoid and slightly dorsoventrally compressed (Figs 13–22). Cells of strain AZA-

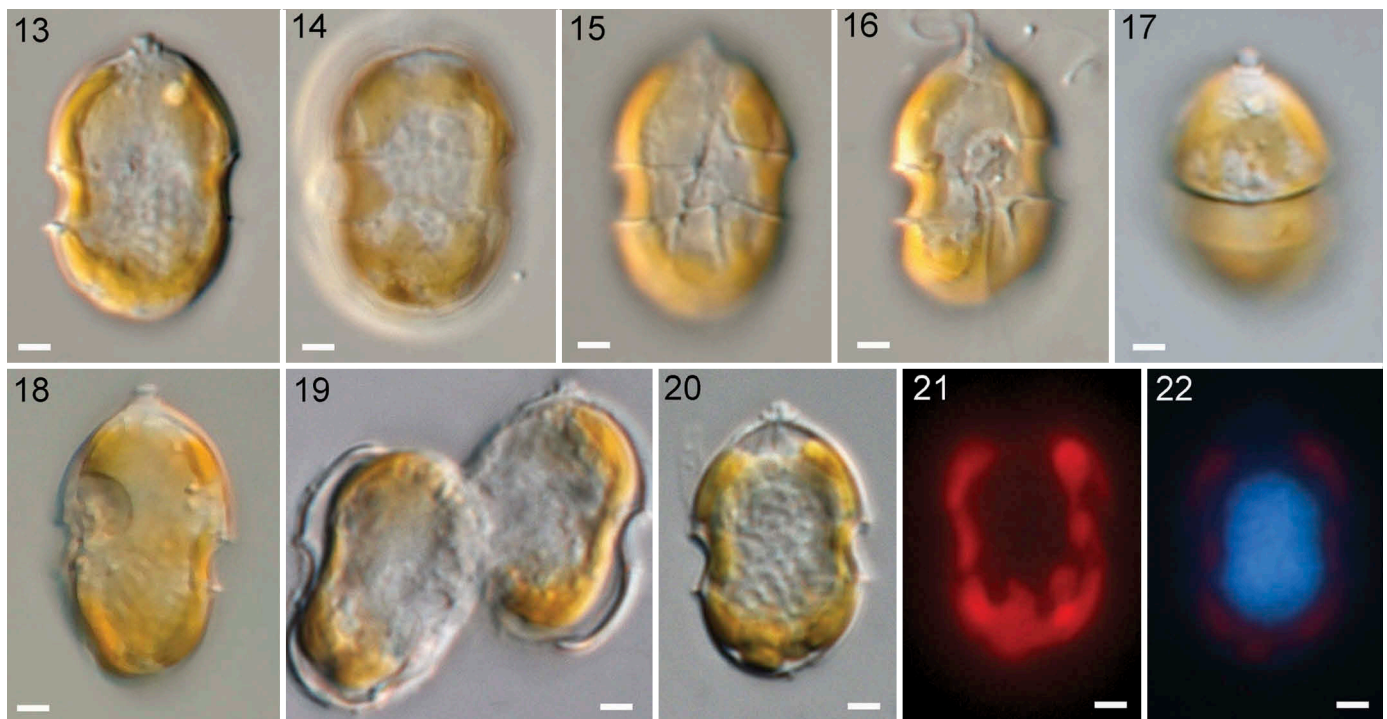
**Table 1.** Strain information. All strains were analysed by light microscopy and scanning electron microscopy. For none of the strains were azaspiracids detected. For all strains, LSU and ITS sequence data were obtained, and for all three *Az. perforatum* strains there are also SSU sequences (see Supplementary Table S3).

Species	Strain	Length (µm)	Width (µm)	l/w ratio	
		Mean ± s Min-max	Mean ± s Min-max	Mean ± s	n
<i>Az. obesum</i>	AZA-1B	15.3 ± 1.0 13.1–17.0	11.6 ± 1.0 9.2–13.8	1.33 ± 0.05	53
<i>Az. obesum</i>	AZA-1C	14.8 ± 0.8 13.2–16.4	10.8 ± 0.8 9.3–12.7	1.37 ± 0.06	53
<i>Az. obesum</i>	AZA-1F	15.8 ± 0.9 13.3–18.0	12.0 ± 0.8 10.2–14.1	1.32 ± 0.05	51
<i>Az. obesum</i>	AZA-1G	14.9 ± 0.9 12.4–16.7	11.0 ± 0.7 9.7–12.4	1.36 ± 0.06	50
<i>Az. obesum</i>	AZA-2B2	14.5 ± 0.9 12.9–16.4	10.7 ± 0.8 9.2–12.8	1.36 ± 0.06	54
<i>Az. obesum</i>	AZA-2D	15.2 ± 0.8 14.0–17.3	11.4 ± 0.9 9.7–13.9	1.34 ± 0.06	53
<i>Az. obesum</i>	AZA-2G	15.6 ± 0.8 13.7–17.1	11.9 ± 0.8 10.6–13.8	1.31 ± 0.05	54
<i>Az. obesum</i>	AZA-ZE4	16.1 ± 1.0 14.1–17.7	12.2 ± 1.1 10.0–14.3	1.32 ± 0.06	53
<i>Az. obesum</i>	AZA-ZE7	16.6 ± 2.3 12.4–22.2	13.3 ± 2.6 8.8–20.0	1.26 ± 0.08	82
<i>Az. obesum</i>	AZA-ZE8	15.3 ± 0.9 13.8–17.5	11.1 ± 0.9 9.7–13.4	1.37 ± 0.06	53
<i>Az. obesum</i>	AZA-ZE9	15.3 ± 1.3 13.2–17.3	11.0 ± 0.8 9.5–12.8	1.40 ± 0.06	52
<i>Az. obesum</i>	AZA-ZE11	15.5 ± 0.9 13.6–17.3	11.8 ± 0.8 10.3–13.6	1.32 ± 0.06	52
<i>Az. trinitatum</i>	AZA-2F	13.7 ± 0.8 12.1–15.4	9.2 ± 0.7 7.6–11.3	1.50 ± 0.08	44
<i>Az. trinitatum</i>	AZA-ZE10	13.5 ± 0.8 12.0–15.9	9.3 ± 0.6 8.1–10.8	1.46 ± 0.07	50
<i>Az. dexteroporum</i>	AZA-2B1	10.5 ± 0.7 9.1–13.2	7.5 ± 0.6 6.5–10.0	1.40 ± 0.06	57
<i>Az. perforatum</i>	AZA-2C	17.6 ± 1.1 14.6–19.2	12.0 ± 0.8 9.9–13.5	1.47 ± 0.05	59
<i>Az. perforatum</i>	AZA-2E	17.8 ± 1.1 15.5–19.5	12.3 ± 0.9 10.4–14.0	1.45 ± 0.06	56
<i>Az. perforatum</i>	AZA-2H	18.0 ± 0.9 15.3–20.0	12.6 ± 0.9 9.9–14.4	1.49 ± 0.07	84

2H had a mean length of 18.0 µm (15.3 to 20.0 µm, n = 84) and a mean width of 12.6 µm (9.9 to 14.4 µm, n = 84), resulting in a mean length:width ratio of about 1.5 (Table 1). The dome-shaped episome terminated in a distinctly acuminate apical pore (Figs 13, 17, 18). The episome was slightly longer than the hemispherical hyposome. The broad cingulum was thus slightly postmedian in position, descending but only slightly displaced (Figs 15, 16).

A single large, lobed and reticulate chloroplast expanded through the entire cell (Figs 13–18, 21) and no indication of a pyrenoid was visible using LM. The large, ellipsoid nucleus was positioned in cell centre (Figs 13, 20, 22). Cytokinesis occurred in motile cells and was of the desmoschisis type in which the parental theca was shared between the two sister cells (Fig. 19).

Thecal plates were thin, but could be clearly observed in light microscopy (Figs 13–20), and were stainable with calcofluor white (not shown). However, because of the delicateness of the plates, the Kofoidian pattern was better resolved by SEM (Figs 23–37, all prepared from the holotype SEM stub).



**Figs 13–22.** *Azadinium perforatum* sp. nov. (strain AZA-2H): LM of living (Figs 13–18) and formaldehyde-fixed (Figs 19–22) cells.

**Figs 13–18.** Living cells showing general size and shape. Scale bars = 2  $\mu$ m.

**Fig. 19.** Formalin fixed cell, late stage of cell division (desmoschisis). Scale bar = 2  $\mu$ m.

**Figs 20–22.** Same cell stained with DAPI in brightfield (Fig. 20), with blue light excitation (Fig. 21) to show chloroplast shape and location, or with UV excitation (Fig. 22) to indicate nuclear shape and location. Scale bars = 2  $\mu$ m.

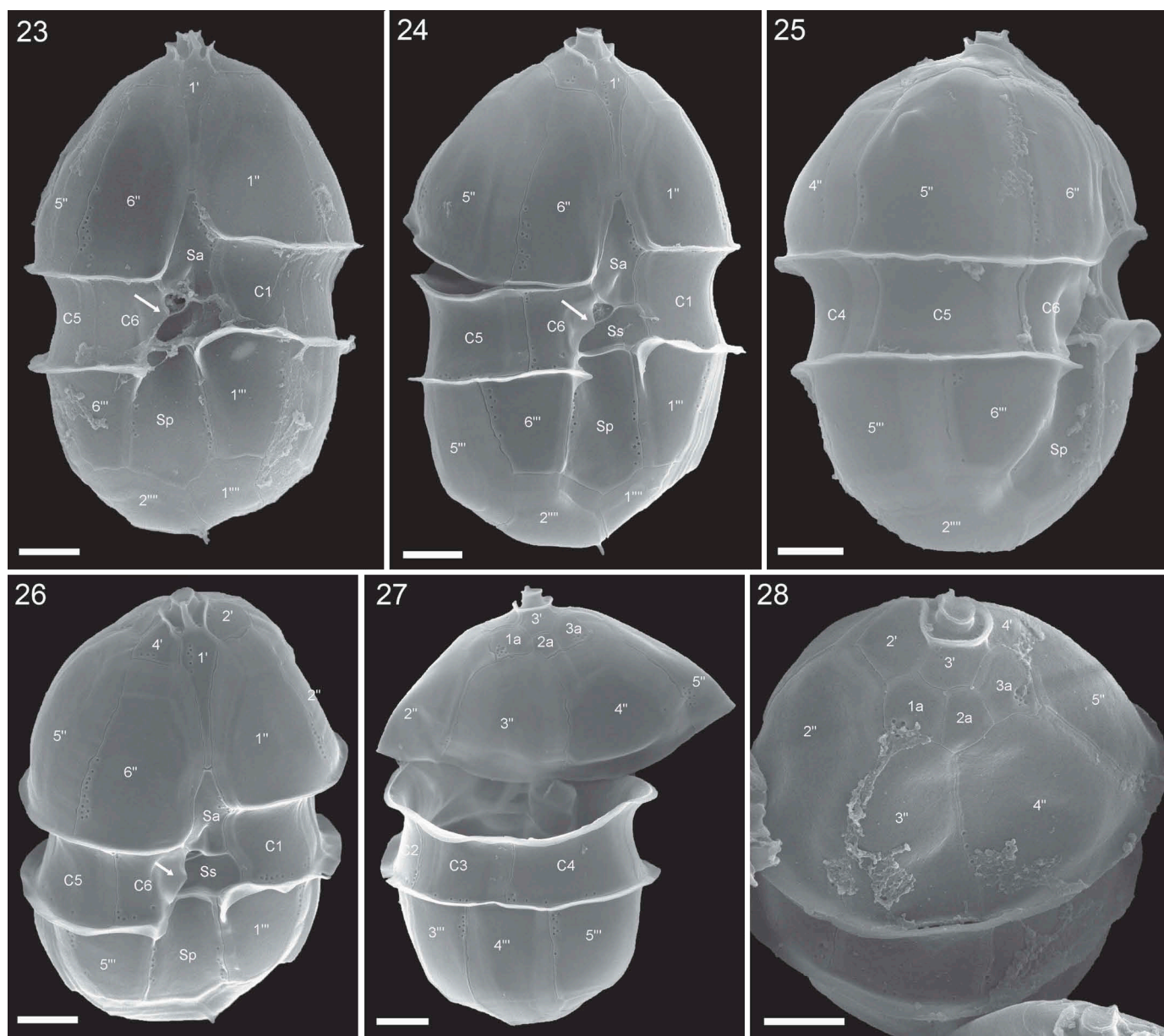
The plate formula was Po, cp, X, 4', 3a, 6'', 6C, 5S, 6''', 2'''' and is schematically drawn in Figs 38–41. Plates were generally smooth, but growth bands of thecal plates were occasionally faintly visible as striated rows running parallel to plate sutures (e.g., Figs 24–27). The presence of these growth bands was restricted to certain sutures.

The acuminate epitheca terminated in the prominent apical pore complex (APC; Figs 23–28) which was composed of three plates: a pore plate (Po) covered by a cover plate (cp), and the canal plate X (Figs 29–31). The pore plate was teardrop-shaped and confined by a collar formed by edges of the apical plates. The collar was narrow and raised, and thus was distinct in LM (Fig. 20). On the tapered ventral side of the pore plate, the collar was open. In the centre of the apical pore plate (Po), a teardrop-shaped pore emerged which was covered by a cover plate (cp). A small X-plate was located where the pore plate abutted the first apical plate. Internal views to determine the exact shape of the X-plate were not obtained. From the exterior, the X-plate had a characteristic three-dimensional structure with finger-like protrusions contacting the apical cover plate (Figs 30, 31). In addition to the APC, the epitheca was composed of 13 thecal plates forming rows of four apical, three anterior intercalary, and six precingular plates (Fig. 29). The six-sided first apical plate was elongated rhomboid or diamond-shaped with a narrow posterior part (Fig. 32). The other three apical plates were small and six-sided, with the dorsal plate 3' being smaller than lateral plates 2' and 4' (Fig. 29). The sutures of plate 3' to its neighbouring apical plates were very short so that the epithecal intercalary plates almost contacted the pore plate. Three small anterior

intercalary plates were symmetrically arranged on the dorsal side of the epitheca (Figs 27, 28, 29, 33) with the middle intercalary plate 2a slightly smaller than the others. All three intercalary plates were five-sided and in contact with two precingular plates. All six precingular plates were of almost equal size, taller than wide, and arranged symmetrically with the suture between plate 3'' and 4'' in mid-dorsal position. Both ventrally-located precingular plates (1'' and 6'') were four-sided, and all other precingulars were five-sided.

The hypotheca was composed of six postcingular and two antapical plates (Fig. 35). Of the six postcingular plates, the two ventrally-located plates were slightly narrower than the other postcingular plates. All postcingular plates were rather long with the lateral and dorsal postcingular plates longer than the two ventral postcingular plates (Figs 23–25). Both antapical plates extended on the dorsal side towards the sulcus. They were different in size with the larger plate 2'''' bearing a minute antapical spine located almost in the middle of the cell close to the suture between plates 1'''' and 2'''' (Figs 23, 24, 35).

The cingulum was wide, about one-fifth of total cell length, and was only slightly displaced by about one-third of its width (Figs 23, 24). There were six cingular plates (Fig. 36). Five of the cingular plates were of comparable size, but the right cingular plate C6 was distinctly narrower and invaded the sulcal area on its left side with an irregularly shaped wing-like extension (arrows in Figs 23, 24, 26). The central sulcal area was deeply concave and the sulcus extended with a slightly concave plate (Sp) along most of the hypotheca. The small central sulcal plates were difficult to resolve because of the internal vaulted structure of the flagellar pore region. Nevertheless, five sulcal plates were



**Figs 23–28.** SEM of *Azadinium perforatum* sp. nov. (strain AZA-2H).

**Fig. 23.** Theca in ventral view. Scale bar = 2  $\mu$ m.

**Figs 24, 25.** Thecae in right lateral view. Scale bar = 2  $\mu$ m.

**Fig. 26.** Theca in apical right lateral view. Scale bar = 2  $\mu$ m.

**Fig. 27.** Theca in dorsal view. Scale bar = 2  $\mu$ m.

**Fig. 28.** Theca in apical dorsal view. Scale bar = 2  $\mu$ m.

identified (Figs 36, 37). The large anterior sulcal plate (Sa) was asymmetrical pentagonal and partly intruded the epitheca with a triangular, tapered anterior part (Figs 23, 24, 26). Two small plates, namely a median sulcal (Sm) and a right sulcal (Sd) plate formed the inverted part of the sulcus (Figs 36, 37). A broad left sulcal plate (Ss) ran horizontally from C1 to C6, thereby separating the posterior sulcal plate (Sp) from the other sulcal plates. The large posterior sulcal plate was approximately twice as long as wide, and triangular at its posterior end (Figs 23–26).

Thecal plates had a limited number of thecal pores of diameter about 0.1  $\mu$ m. On precingular, cingular, and post-cingular plates the pores were arranged mainly as rows

parallel to some plate sutures (Figs 23–28). The first apical plate had a characteristic anterior row of five to ten pores (Figs 29, 30, 32), whereas pores on other apical and intercalary plates were scattered and ranged from zero to eight pores per plate (Figs 29, 33). The median intercalary plate 2a was usually free of pores, but occasionally one pore occurred (Figs 29, 33). Dorsal plates 3'' and 4''' of the pre- and post-cingular series were free of pores. A few small pores were present on the second antapical plate, whereas the first antapical plate had no pores (Fig. 35). Some pores were consistently present on all three larger sulcal plates, i.e., on Sa, Ss and Sp (Figs 23, 24, 26).





**Figs 29–37.** *Azadinium perforatum* sp. nov. (strain AZA-2H): SEM micrographs of different cells to illustrate epithelial plate arrangement.

**Fig. 29.** Apical view. Scale bar = 2  $\mu$ m.

**Fig. 30.** Detailed view of apical pore complex in central view. Scale bar = 1  $\mu$ m.

**Fig. 31.** Detailed view of apical pore complex in apical view. Scale bar = 0.5  $\mu$ m.

**Fig. 32.** Ventral view of first apical plate. Scale bar = 1  $\mu$ m.

**Figs 33, 34.** Detailed dorsal view of apical and anterior intercalary plates. Note Fig. 34 suggests that plate 3' and 2a are fused. Scale bars = 1  $\mu$ m.

**Fig. 35.** Antapical view of hypothecal plates. Scale bar = 2  $\mu$ m.

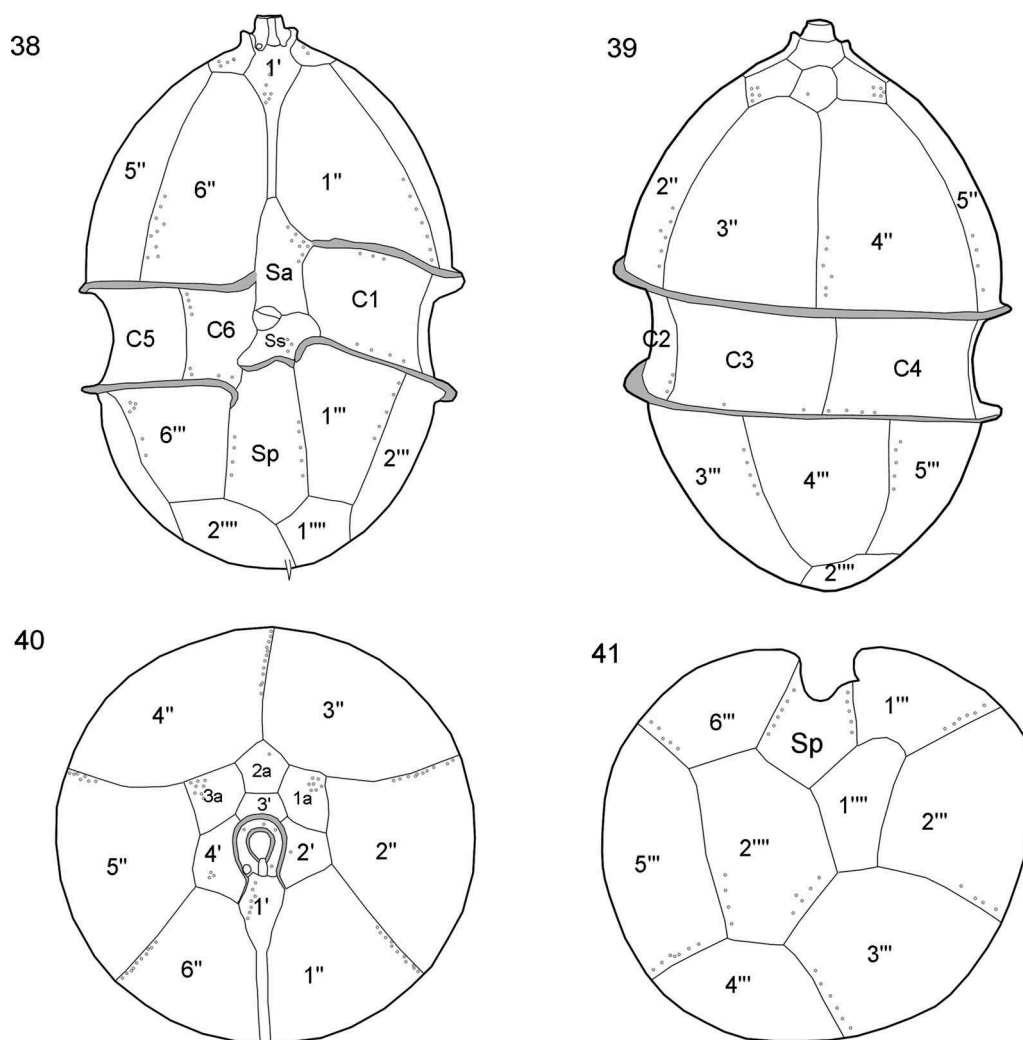
**Fig. 36.** Dorsal/apical view of hypotheca showing series of cingular plates with interior view of sulcal plates. Scale bar = 2  $\mu$ m.

**Fig. 37.** Details of sulcal plate arrangement in external view. Scale bar = 1  $\mu$ m.

The plate pattern shown in Figs 38–41 was standard; however, some variation occurred in culture. A common (but not quantified) variation was the lack of a suture between plates 3'

and 2a, leading to a single elongated dorsal apical plate extending posteriorly between, and separating the two remaining anterior intercalary plates (Fig. 34).





**Figs 38–41.** *Azadinium perforatum* sp. nov. Schematic illustrations of tabulation. Plate labels according to Kofoidian system. Positions of thecal pores indicated in Figs 38–41 as small grey circles; position of small antapical spine indicated in Fig. 38.

**Fig. 38.** Ventral view.

**Fig. 39.** Dorsal view.

**Fig. 40.** Apical view.

**Fig. 41.** Antapical view.

## Morphology of other strains

### *Azadinium obesum* Tillmann & Elbrächter

Figs 42–52

With 12 new strains, *Azadinium obesum* (Figs 42–52) was the species most often obtained from single-cell isolation at station 1. All strains of *Az. obesum* shared identical morphology in LM and SEM. No pyrenoid was visible using light microscopy (Figs 42–44). SEM revealed the Kofoidian plate pattern, Po, cp, X, 4', 3a, 6'', 6C, 5S, 6''', 2''', and plate size and arrangement as described for the type species (Figs 46–52). As a distinctive morphological feature, the ventral pore was located on the left margin of plate 1' (Figs 46, 50). For all strains of *Az. obesum*, plate 2a was present in both quadra- (i.e. in contact with one precingular plate) and penta-configuration (in contact with two precingular plates; Figs 49, 50). Epithecal intercalary plates

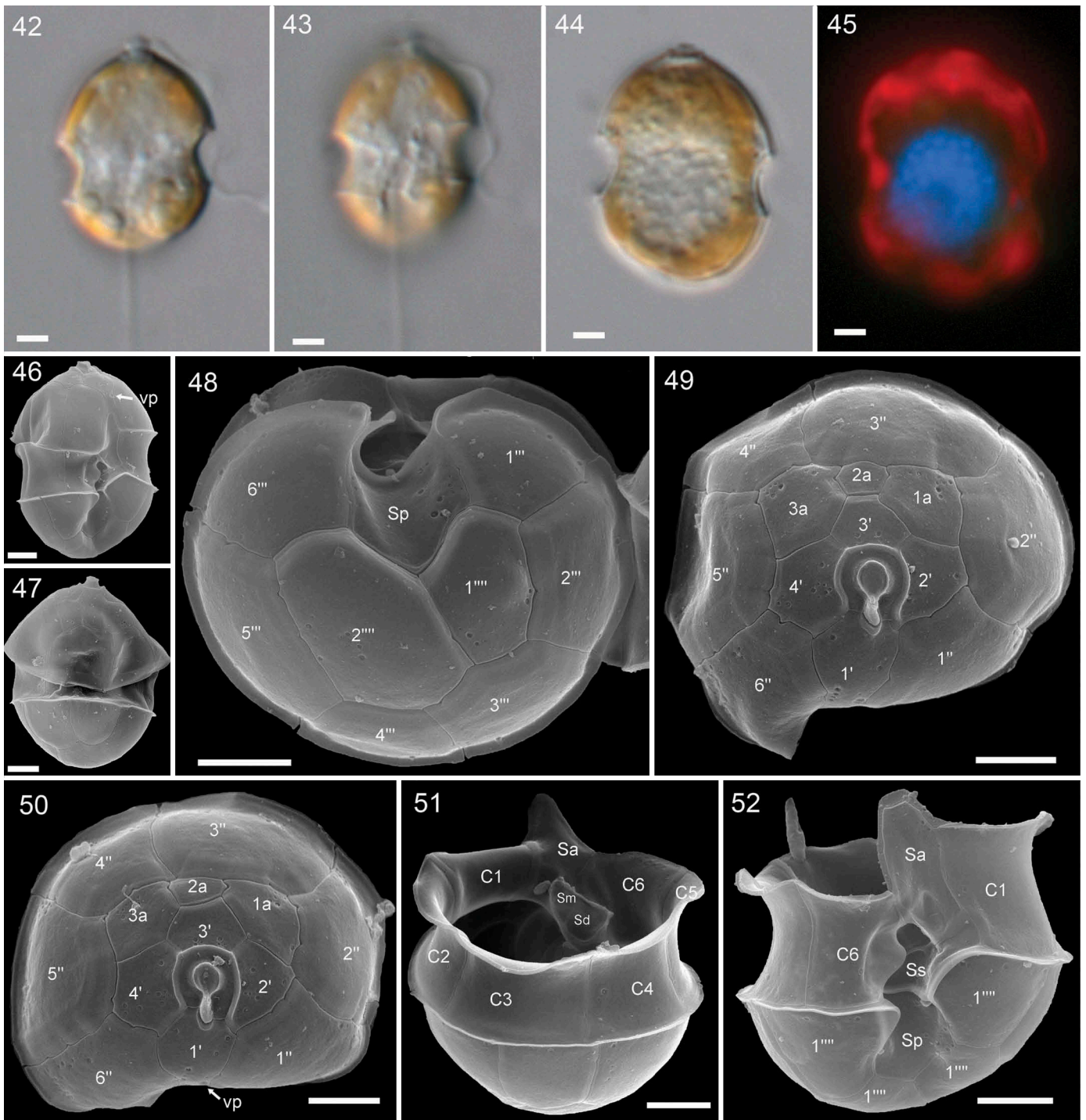
were relatively small, and the first (1a) was not in contact with plate 1'' (Figs 49, 50).

### *Azadinium dexteroporum* Percopo & Zingone

Figs 53–62

One strain was identified as *Azadinium dexteroporum* (Figs 53–62). Cells of strain AZA-2B1 were distinctly smaller than other strains (Table 1). In LM, the very broad and excavated cingulum, acuminate apex, distinct antapical spine, and relatively small pyrenoid visible by its starch cup, were observed (Figs 53–55). Dividing cells retained their motility throughout mitosis and cytokinesis, the latter being of the desmoschisis type, i.e., parental theca shared by the two sister cells (Fig. 56).

The Kofoidian plate pattern and most plate details (Figs 57–62) conformed to the species description. The distinctly smaller central intercalary plate 2a was quadrangular



**Figs 42–52.** Light and scanning electron micrographs of *Azadinium obesum* (strain AZA-2D). vp, ventral pore.

**Figs 42, 43.** LM, living cells in ventral view. Scale bars = 2  $\mu$ m.

**Figs 44, 45.** Formalin fixed cells in brightfield (Fig. 44) or with calcofluor staining and epifluorescence (UV excitation; Fig. 45) to illustrate shape and location of nucleus (blue) and chloroplast (red). Scale bars = 2  $\mu$ m.

**Fig. 46.** SEM of theca in ventral view. Scale bar = 2  $\mu$ m.

**Fig. 47.** SEM of theca in dorsal view. Scale bar = 2  $\mu$ m.

**Fig. 48.** Hypothecal plates in antapical view. Scale bar = 2  $\mu$ m.

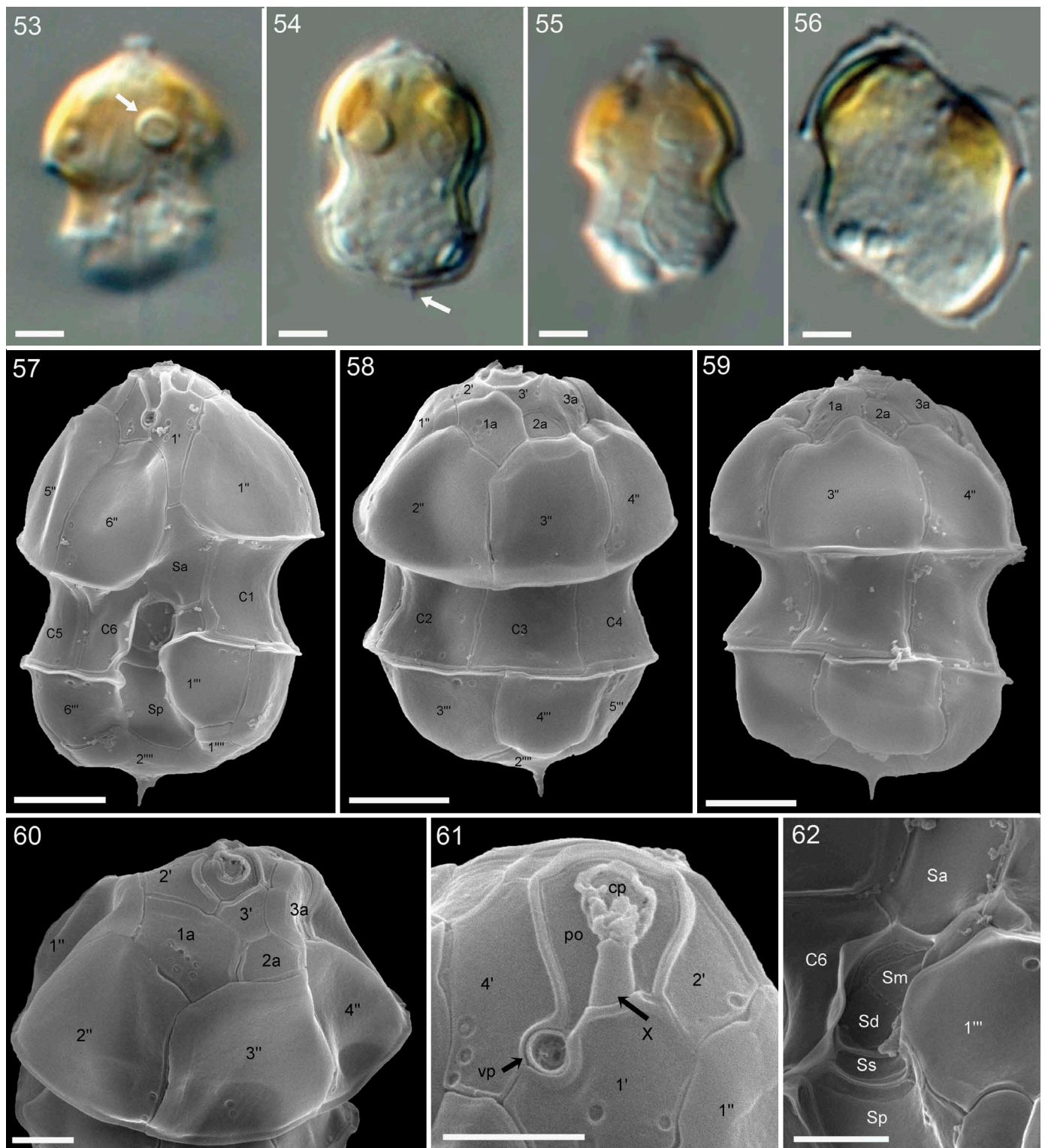
**Figs 49, 50.** Epithelial plates in apical view. Note plate 2a in quadra (Fig. 49) or penta (Fig. 50) configuration. Scale bars = 2  $\mu$ m.

**Fig. 51.** Dorsal/apical view of hypotheca showing series of cingular plates with an interior view of sulcal plates. Scale bar = 2  $\mu$ m.

**Fig. 52.** Hypotheca in ventral view showing details of sulcal plates. Scale bar = 2  $\mu$ m.

and often almost symmetrically located above plate 3" (Figs 58, 60). However, a penta-configuration (i.e., plate 2a was pentagonal) was also present, with plate 2a contacting plates 3" and 4" (Figs 58, 59). Different from the Mediterranean type

strain, plate 2a of the Labrador Sea strain (AZA-2B1) was not concave, although at times the thick plate overgrowth of adjoining plates gave a slightly sunken appearance to this plate (Fig. 58). As the most characteristic feature, the ventral



**Figs 53–62.** Light and scanning electron micrographs of *Azadinium dexteroporum* (strain AZA-2B1). cp, cover plate; X, X-plate; vp, ventral pore; po, pore plate.  
**Figs 53–56.** LM, living cells showing general size and shape, one pyrenoid (arrow in Fig. 53) in episome, and presence of an antapical spine (arrow in Fig. 54). Scale bars = 2  $\mu$ m.  
**Fig. 56.** Dividing cell in late stage of desmoschisis. Scale bar = 2  $\mu$ m.  
**Fig. 57.** SEM of theca in ventral view. Scale bar = 2  $\mu$ m.  
**Figs 58, 59.** SEM of thecae in or dorsal view. Note plate 2a in quadra (Fig. 58) or penta (Fig. 59) configuration. Scale bars = 2  $\mu$ m.  
**Fig. 60.** Detailed dorsal view of apical area showing a plain plate 2a. Scale bar = 1  $\mu$ m.  
**Fig. 61.** Detailed view of apical pore complex showing position of ventral pore. Scale bar = 1  $\mu$ m.  
**Fig. 62.** Details of sulcal plate arrangement in external view. Scale bar = 1  $\mu$ m.

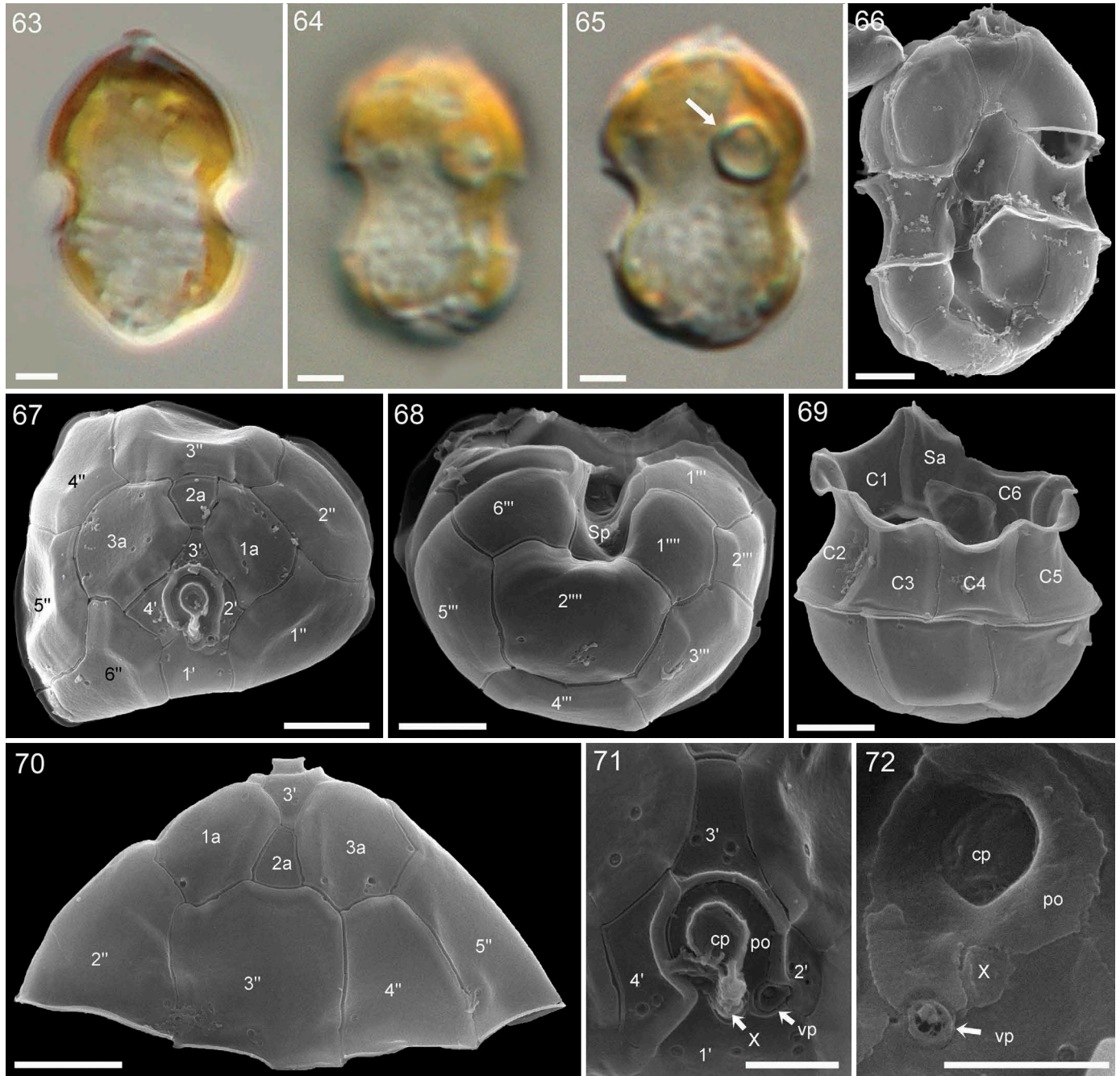


pore (vp) was located at the distal end of the somewhat elongated right side of the asymmetric pore plate (Fig. 61). As has been observed in the central sulcal region of the type strain, occasionally an additional structure was visible above Sm and Sd (Fig. 62). However, it could not be verified if this represented an additional sulcal platelet, or an internal outgrowth of plate C6 extending to both central sulcal plates.

*Azadinium trinitatum* Tillmann & Nézan

Figs 63–72

Two strains of *Azadinium trinitatum* (AZA-2F, AZA-ZE10) were obtained. Cells varied in shape with an epitheca ranging from conical to more dome-shaped. Viewed by LM (Figs 63–65), one pyrenoid was located in the episome. SEM examination



**Figs 63–72.** Light and scanning electron micrographs of *Azadinium trinitatum* (strain AZA-2F). cp, cover plate; X, X-plate; vp, ventral pore; po, pore plate.

**Figs 63–65.** LM, living cells showing general size and shape, and one pyrenoid (arrow in Fig. 65) in episome. Scale bars = 2  $\mu$ m.

**Fig. 66.** SEM of theca in ventral view. Scale bar = 2  $\mu$ m.

**Fig. 67.** Epithecical plates in apical view. Scale bar = 2  $\mu$ m.

**Fig. 68.** Hypothecal plates in antapical view. Scale bar = 2  $\mu$ m.

**Fig. 69.** Dorsal view of hypotheca showing series of cingular plates with an interior view of sulcal plates. Scale bar = 2  $\mu$ m.

**Fig. 70.** Epitheca in dorsal view. Scale bar = 2  $\mu$ m.

**Fig. 71.** Detailed view of apical pore complex in external view. Scale bar = 1  $\mu$ m.

**Fig. 72.** Detailed view of apical pore complex in internal view. Scale bar = 1  $\mu$ m.



(Figs 66–72) showed most morphological details described for the type strain, i.e., presence of relatively small apical plates, a broad contact of plates 1a and 1", and a ventral pore located at the left lateral side of the pore plate in a cavity of the 1' plate at the tip of an elongated side of a slightly asymmetric pore plate. However, different from the type strain from Iceland, both cultured strains from the Labrador Sea lacked any indication of an antapical spine on plate 2'''.

### AZA analysis strains

All strains tested were negative for AZA. The limits of detection (LOD) in the SRM mode for the targeted analysis of known AZA ranged between 0.7 and 23 ag cell<sup>-1</sup>, depending on analysed biomass. LOD in the less sensitive precursor ion mode for the search of unknown AZA variants ranged between 29 and 596 ag cell<sup>-1</sup> (Table S2).

### Sequence data and phylogeny

Three strains of *Az. perforatum* (AZA-2C, -2E, -2H) shared identical SSU rDNA sequences.

For LSU rDNA sequence comparison, *Az. dexteroporum* strain AZA-2B1 shared identical sequences with strain 1-D12 and differed from the type strain at nine positions (92.54% similarity for 624 bp). The AZA-ZE10 strain of *Az. trinitatum* differed from AZA-2F at three positions (99.60% similarity, out of 742 bp) and differed from N-39-04 at five positions (99.33% similarity, for 742 bp). Various strains of *Az. obesum* (AZA-1B, -1F, -2B2, -2D, -2G, -ZE8, -ZE9) and the type strain 2E10 shared identical sequences, and strains AZA-1C, -1G, -ZE7 shared identical sequences, too. They differed from each other at three positions (99.59% similarity, for 730 bp). *Az. perforatum* strains AZA-2C and -2H shared identical sequences and differed from AZA-2E at only one position (99.84% similarity, for 619 bp).

For ITS rDNA sequence comparison, *Az. dexteroporum* strain AZA-2B1 differed from strain 1-D12 at one position (99.81% similarity, for 529 bp) and from the type strain at 23 positions (95.60% similarity, for 529 bp). Strain *Az. trinitatum* (AZA-ZE10) differed from AZA-2F at three positions (99.45% similarity, for 544 bp) and differed from N-39-04 at four

positions (99.26% similarity, for 544 bp). Various strains of *Az. obesum* (AZA-1F, -2D, -2G, -ZE4, -ZE8, -ZE9) and the type strain 2E10 had identical sequences as did strains AZA-1C, -1G. They differed at three positions (99.46% similarity, for 560 bp). *Az. perforatum* strain AZA-2H differed from AZA-2C and -2E at three and four positions (99.51% and 99.35% similarity, for 616 bp). Uncorrected pairwise genetic distances for selected *Azadinium* and *Amphidoma* strains and species based on ITS rDNA sequences ranged from 0.002 to 0.319 (Table 2).

Maximum likelihood (ML) and Bayesian inference (BI) analysis based on combined SSU, ITS and partial LSU rDNA sequences yielded similar phylogenetic trees. The BI tree is illustrated in Fig. 73. The family Amphidomataceae was well resolved with moderate support (0.75 BPP/100 BS). The new species *Az. perforatum* was monophyletic with maximal support (1.0 BPP/100 BS) and was a sister clade to *Amphidoma parvula* and *Am. languida* with strong support (0.97 BPP/100 BS). The group diverged earlier than other species of Amphidomataceae, followed by *Azadinium concinnum*, with moderate support (0.7 BPP/100 BS). All other *Azadinium* species grouped with moderate support (0.82 BPP/100 BS). *Azadinium dexteroporum* strain AZA-2B1 grouped with strain 1-D12 with maximal support, which was a sister clade to the type strain from Italy. Both new *Az. trinitatum* strains (AZA-ZE10 and -2F) grouped with maximal support, and made a sister clade of strains from Norway and Iceland, with maximal support. All *Az. obesum* strains grouped with maximal support. The group consisted of two clades formed by strains from the North Atlantic Ocean with strong support (0.94 BPP/100 BS and 0.99 BPP/100 BS, respectively), and a third clade was formed by a strain from northeast Pacific Ocean.

### *Azadinium* spp. in the Labrador Sea field sample

Figs 74–109

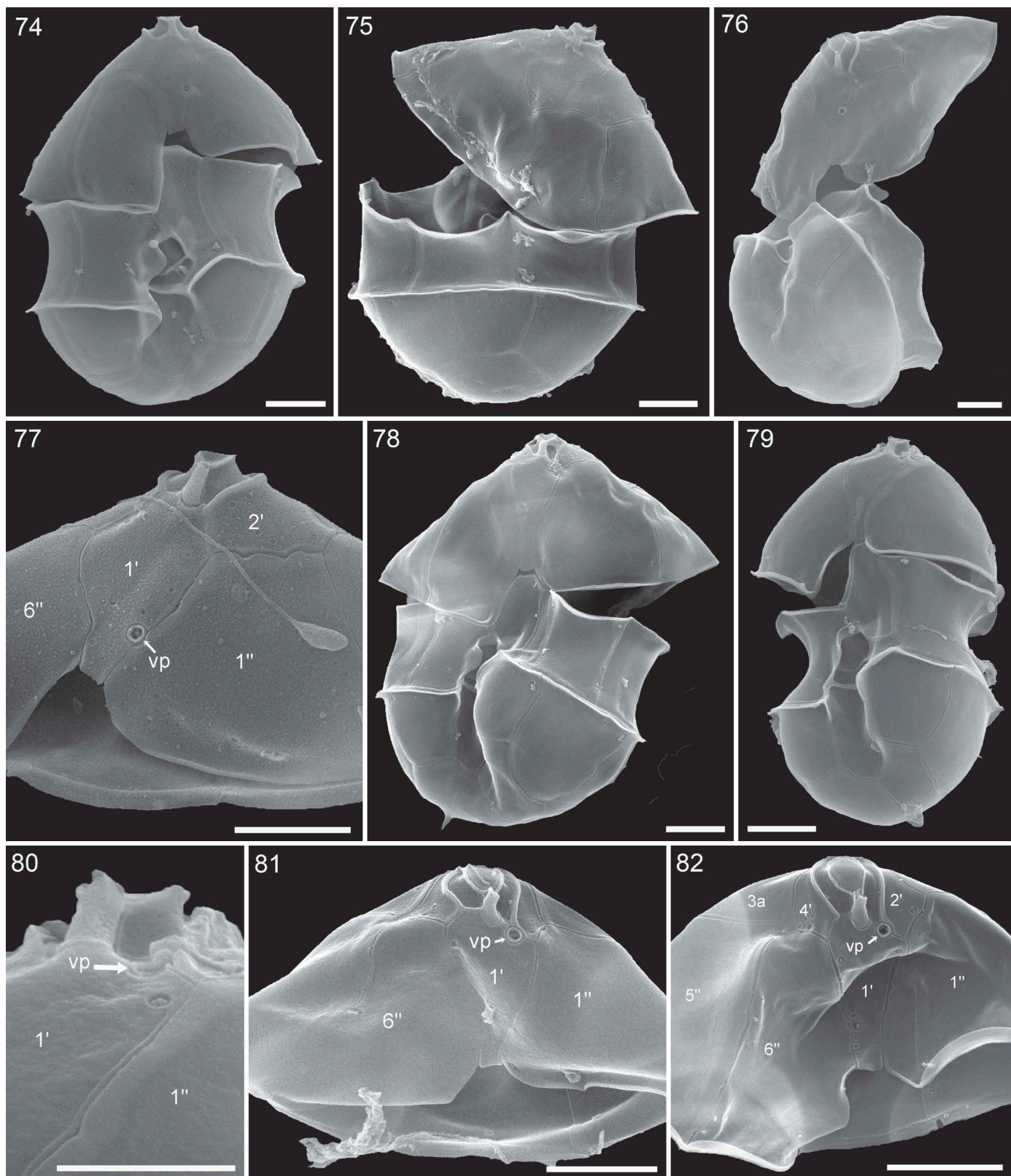
SEM analysis of the concentrated formaldehyde-fixed bottle sample of station 1 in the central Labrador Sea confirmed the presence of species for which culture strains were obtained, i.e. *Az. perforatum*, *Az. dexteroporum*, *Az. obesum* and *Az. trinitatum*. Cells of *Az. obesum* in the field sample were most easily

**Table 2.** Uncorrected genetic *p*-distance between ITS rDNA sequences of some selected *Azadinium*/*Amphidoma* species/strains. Asterisks (\*) denote strains obtained in this study.

	<i>Az. dexteroporum</i> AZA-2B1*	<i>Az. dexteroporum</i> (type)	<i>Az. obesum</i> AZA-1G*	<i>Az. obesum</i> 2E10	<i>Az. trinitatum</i> AZA-2F*	<i>Az. trinitatum</i> 4B11	<i>Az. concinnum</i> 1C6	<i>Az. perforatum</i> AZA-2H*	<i>Am. languida</i> SM1	<i>Am. parvula</i> H-1E9
<i>Az. dexteroporum</i> AZA-2B1*	-									
<i>Az. dexteroporum</i> (type)	0.038	-								
<i>Az. obesum</i> AZA-1G*	0.143	0.146	-							
<i>Az. obesum</i> 2E10	0.142	0.144	0.002	-						
<i>Az. trinitatum</i> AZA-2F*	0.151	0.156	0.055	0.053	-					
<i>Az. trinitatum</i> 4B11	0.150	0.154	0.047	0.046	0.006	-				
<i>Az. concinnum</i> 1C6	0.276	0.261	0.251	0.253	0.250	0.250	-			
<i>Az. perforatum</i> AZA-2H*	0.270	0.277	0.258	0.258	0.277	0.272	0.293	-		
<i>Am. languida</i> SM1	0.295	0.286	0.290	0.292	0.294	0.293	0.277	0.325	-	
<i>Am. parvula</i> H-1E9	0.312	0.302	0.307	0.309	0.319	0.317	0.285	0.295	0.206	-







**Figs 74–82.** SEM, field sample from station 1. vp, ventral pore.

**Fig. 74.** *Azadinium obesum* in ventral view. Scale bar = 2  $\mu$ m.

**Fig. 75.** *Azadinium obesum* in dorsal view. Scale bar = 2  $\mu$ m.

**Fig. 76.** Unfolded thecae of *Az. obesum* allowing antapical/lateral view of hypotheca and ventral view of epitheca. Scale bar = 2  $\mu$ m.

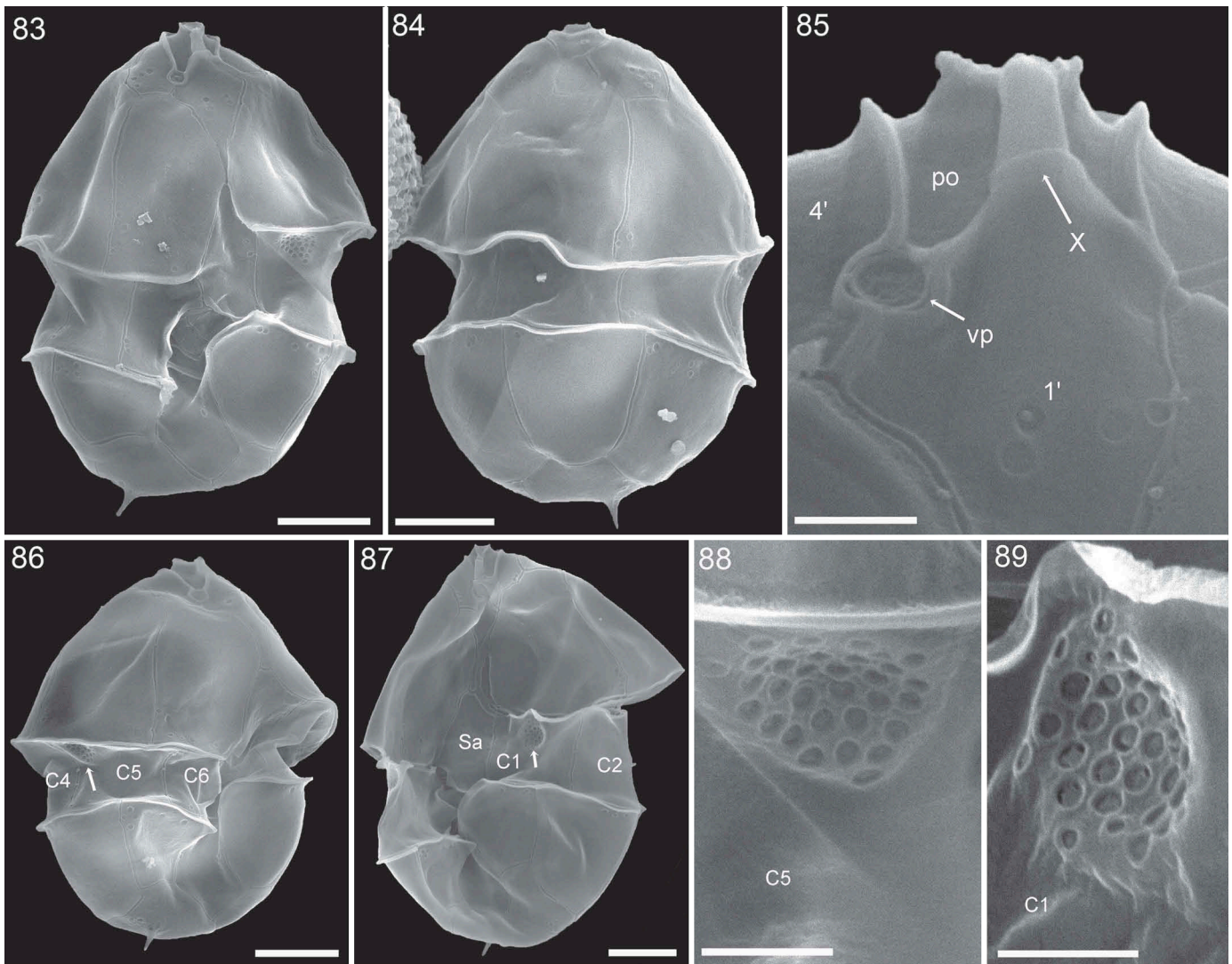
**Fig. 77.** Epitheca of *Azadinium obesum* in ventral view showing position of ventral pore. Scale bar = 2  $\mu$ m.

**Figs 78, 79.** *Azadinium trinitatum* in ventral view. Note presence (Fig. 78) or absence (Fig. 79) of antapical spine. Scale bars = 2  $\mu$ m.

**Fig. 80.** Detailed apical view of cell shown in Fig. 79 indicating position of ventral pore. Scale bar = 1  $\mu$ m.

**Figs 81, 82.** Epitheca of *Azadinium trinitatum* in ventral view showing position of ventral pore and small lateral apical plates. Scale bars = 2  $\mu$ m.





**Figs 83–89.** SEM, field sample from station 1, *Azadinium dexteroporum*. X, X-plate; vp, ventral pore; po, pore plate.

**Fig. 83.** Cell in ventral view. Scale bar = 2  $\mu$ m.

**Fig. 84.** Cell in dorsal view. Scale bar = 2  $\mu$ m.

**Fig. 85.** Detailed view of apical pore complex showing position of ventral pore. Scale bar = 0.5  $\mu$ m.

**Figs 86, 87.** Cells in ventral view indicating position of pore fields (arrows) on cingular plates C5 (Fig. 86) and C1 (Fig. 87). Scale bars = 2  $\mu$ m.

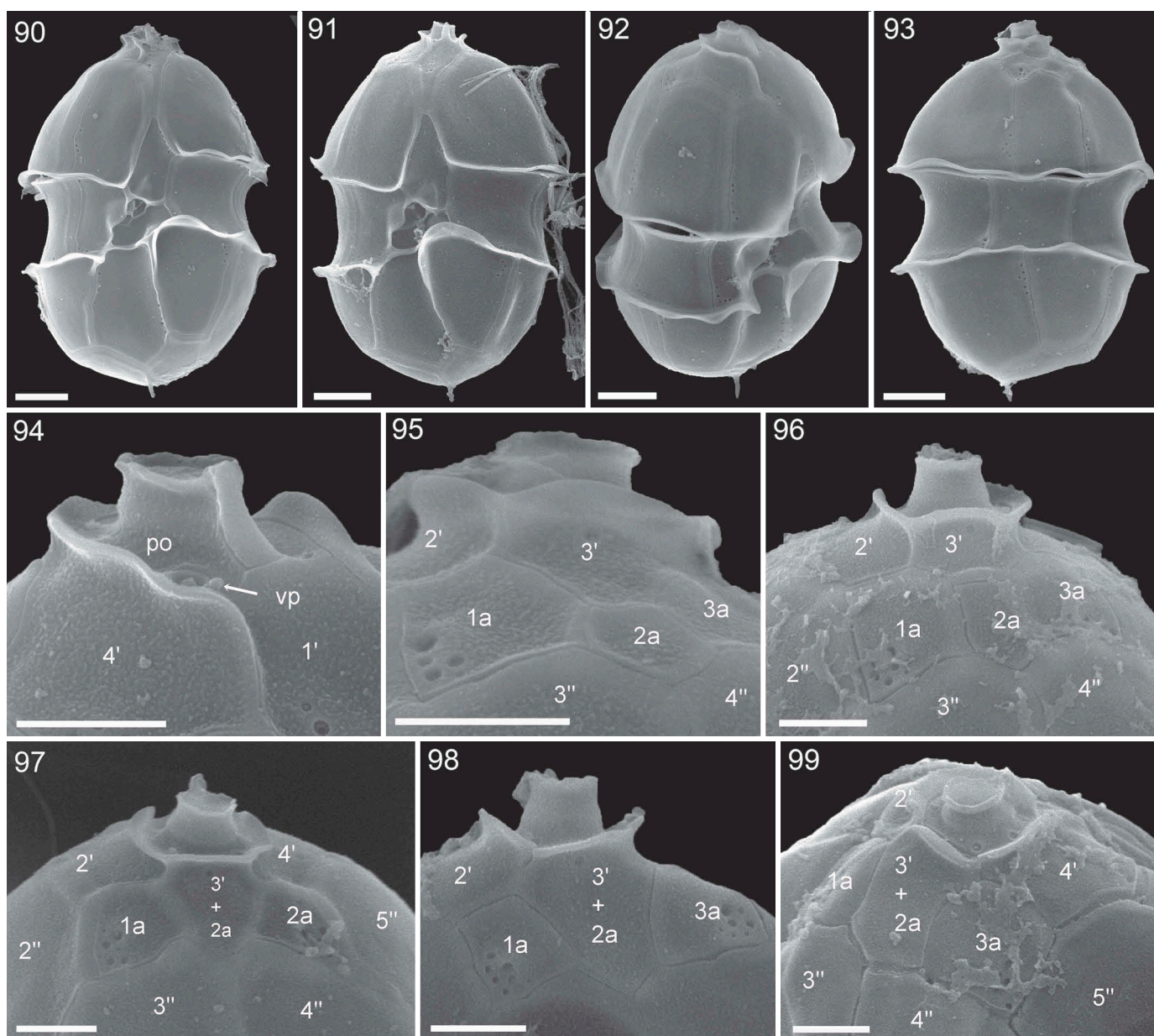
**Figs 88, 89.** Detailed view of cingular pore fields. Scale bars = 0.5  $\mu$ m.

identified by shape, position of ventral pore, by lack of a spine, and the small anterior intercalary plates with the missing contact of plates 1a and 1" (Figs 74–77). Identifying specimens of *Az. trinitatum* (Figs 78–82) was difficult and required simultaneous visibility of both the ventral pore and the narrow apical plates to differentiate the species from *Az. poporum* and *Az. dalianense*. Most cells identified as *Az. trinitatum* lacked a spine (Fig. 79), but a single cell with a spine, likely representing *Az. trinitatum*, was observed (Fig. 78). Cells of *Az. dexteroporum* (Figs 83–89) were easily detected by their small size and peculiar position of the ventral pore. All cells attributed to *Az. dexteroporum* in dorsal view had a plane median intercalary plate 2a (Fig. 84). Cells of the field sample had a conspicuous roundish field of thecal pores on cingular plates C1 and C5 (Figs 86–89). Specimens of the new species *Az. perforatum* (Figs 90–99) were regularly observed in the field sample, and these conformed to the morphological description of strain

AZA-2H. Just as for cells of the isolated strains, specimens of field samples were observed with fused dorsal apical plates 3' and 2a (Figs 97–99).

In addition to species confirmed by established strains, additional species were identified. A single specimen of *Az. spinosum* was recorded based on presence of a spine and position of the ventral pore (Figs 100, 101). With ventral pore position resembling *Az. spinosum*, but with an elongated pore plate and large lateral apical plates, a few cells were identified as *Az. polongum* Tillmann (Figs 102, 103). Although appearing wrinkled and unfortunately blurred in SEM, two cells were identified as *Am. languida* based on the ventral pore position (Figs 104, 105) or by the presence of an antapical pore (Fig. 106). Moreover, a number of epithelial cell fragments were observed where apical plate number and arrangement conformed to *Az. dalianense* Z. Luo, H. Gu & Tillmann, but where the position of the





**Figs 90–99.** SEM, field sample of station 1, *Azadinium perforatum* sp. nov. vp, ventral pore; po, pore plate.

**Figs 90, 91.** Cells in ventral view. Scale bars = 2  $\mu$ m.

**Fig. 92.** Cell in left lateral view. Scale bar = 2  $\mu$ m.

**Fig. 93.** Cell in dorsal view. Scale bar = 2  $\mu$ m.

**Fig. 94.** Detailed view of apical pore complex showing position of ventral pore. Scale bar = 1  $\mu$ m.

**Figs 95–99.** Detailed dorsal view of apical area. Note suture between plates 3' and 2a in Figs 95 and 96, which is missing in 97–99. Scale bars = 1  $\mu$ m.

ventral pore was distinct, and located on the suture of plates 1' and 2' (Figs 107–109). Whole cell views of such cells were not available, and further observation is needed to characterise this potential new species.

## DISCUSSION

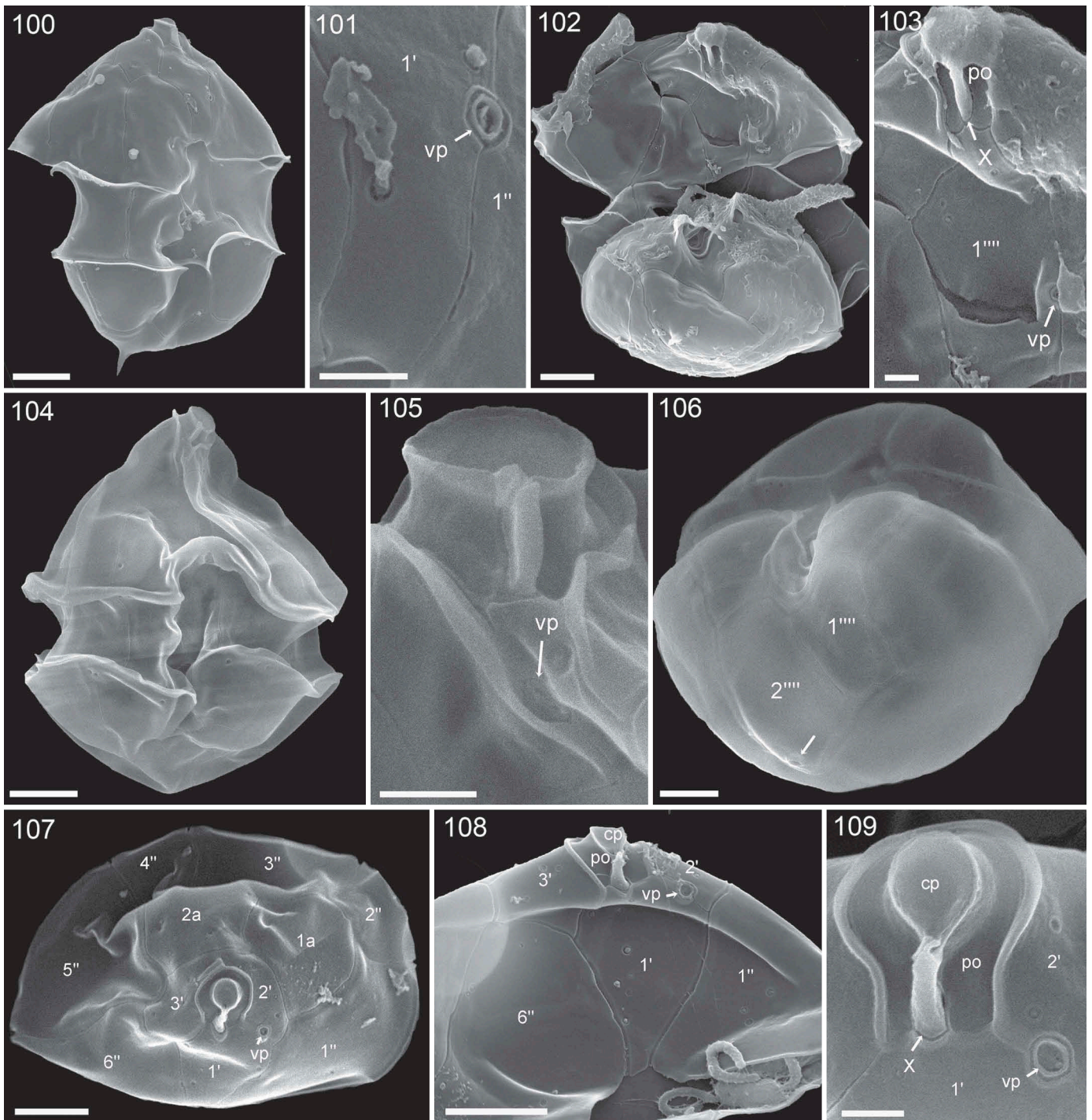
In the first study of Amphidomataceae in subarctic areas (Tillmann *et al.* 2014a), seven randomly isolated strains represented as many as five species, three of which were newly described. With the present study and the description of

a new *Azadinium* species, we demonstrate that the biodiversity of Amphidomataceae in the subarctic is remarkably large.

### *Azadinium perforatum* sp. nov.

Morphological and molecular sequencing approaches clearly show that three of the newly established strains from the Labrador Sea represent a new species. The new taxon belongs to the genus *Azadinium* as it conforms to all features described as characteristic for the genus, including the plate pattern with four apical and three epithecal intercalary plates, both six post- and precingular plates, and two antapical plates





**Figs 100–109.** SEM, field sample of station 1. cp, cover plate; X, X-plate; vp, ventral pore; po, pore plate.

**Fig. 100.** *Azadinium spinosum* in ventral view. Scale bar = 2  $\mu$ m.

**Fig. 101.** *Azadinium spinosum*. Detailed view of the ventral area of the same cell shown in Fig. 100 to illustrate the position of the ventral pore. Scale bar = 0.5  $\mu$ m.

**Fig. 102.** *Azadinium polongum* in ventral view. Scale bar = 2  $\mu$ m.

**Fig. 103.** Detailed view of cell in Fig. 102 showing position of ventral pore and shape of the pore plate. Scale bar = 0.5  $\mu$ m.

**Fig. 104.** *Amphidoma languida* in ventral view. Scale bar = 2  $\mu$ m.

**Fig. 105.** Detailed view of cell in Fig. 104 showing position of ventral pore.

**Fig. 106.** *Amphidoma languida* in ventral/antapical view showing position of antapical pore (arrow). Scale bar = 2  $\mu$ m.

**Figs 107–109.** Epithecae of *Azadinium* sp. in ventral/apical view. Note peculiar position of ventral pore located in middle of suture of plates 1' and 2', and presence of three apical plates and two anterior intercalary plates. Scale bars = 2  $\mu$ m (107, 108) and 0.5  $\mu$ m (109).

(Tillmann et al. 2009). Although *Az. perforatum* resembles several other species of *Azadinium* in size and overall shape, it possesses a distinctive and unique combination of features,

which unambiguously differentiate this species from others (Table 3). Previous work on *Azadinium* and *Amphidoma* emphasised that the position of the ventral pore (vp) is

**Table 3.** Compilation of morphological features of species of *Azadinium* (including *Az. perforatum*) with a ventral pore located at the right side of the pore plate.

	<i>Az. caudatum</i> var. <i>margalefii</i>	<i>Az.</i> <i>dexteroporum</i>	<i>Az.</i> <i>concinnum</i>	<i>Az.</i> <i>luciferelloides</i>	<i>Az.</i> <i>zhuanum</i>	<i>Az.</i> <i>perforatum</i>
Length range $\mu\text{m}$ (mean)	25.0–42.1	7.0–10.0 (8.5)	8.0–11.5 (9.5)	9.4–14.1 <sup>†</sup> (11.1)	16.8–21.6 (18.5)	15.3–20.0 (18.0)
Width range $\mu\text{m}$ (mean)	18.4–30.0	5.0–8.0 (6.2)	5.6–8.3 (6.6)	6.6–10.1 <sup>†</sup> (7.9)	12.5–18.8 (14.8)	9.9–14.4 (12.6)
L/W ratio	1.2	1.4	1.4	1.4	1.3	1.5
Antapical projection	short horn, long spine	spine	spine	spine	spine	tiny spine
Stalked pyrenoid	none	1	none	unknown	1	none
1'' in contact 1a	yes	yes	no	yes	yes	no
Number of apicals and intercalary plates	4, 3	4, 3	4, 3	4, 3	3, 2	4, 3
Ventral pore position	pore plate, right side, inside Po	end of pore plate, right side	pore plate, right side	pore plate, right side	pore plate, right side	pore plate, right side
Pore plate symmetry	suture to 1' almost symmetric	suture to 1' strongly asymmetric, left side more apical	suture to 1' almost symmetric	suture to 1' almost symmetric	suture to 1' almost symmetric	suture to 1' almost symmetric
Thecal pores on pore plate	no	no	no	no	no	yes
Relative size of first and last intercalary	small	small	very small	small	large	small
Relative size of apical plates	medium	small	small	small	medium	medium
Size and arrangement of precingular plates	Plate 3'' mid-dorsal, plates 2'' and 4'' small	Plate 3'' mid-dorsal	Large, symmetrically arranged, plate 3'' and 4'' mid-dorsal	Plate 3'' mid-dorsal	Plate 3'' mid-dorsal	Large, symmetrically arranged, plate, 3'' and 4'' mid-dorsal
Records	Mediterranean, North Sea, Atlantic	Mediterranean, North Atlantic, South Atlantic	North Atlantic	South Atlantic	East China Sea, Yellow Sea	Labrador Sea
Reference <sup>‡</sup>	a, b	c, d	e	f	g	This study

<sup>†</sup> Based on SEM only. <sup>‡</sup> a, Nézan *et al.* (2012); b, Tillmann *et al.* (2014b); c, Percopo *et al.* (2013); d, Tillmann *et al.* (2015); e, Tillmann *et al.* (2014a); f, Tillmann & Akselmann (2016); g, Luo *et al.* (2017)

diagnostic for species discrimination, although two new species of *Amphidoma*, *Am. parvula* Tillmann & Gottschling and *Am. alata* Tillmann, lack such a ventral pore (Tillmann 2018a; Tillmann *et al.* 2018b). The amphidomatacean vp is larger than regular thecal pores, surrounded by a platelet-like structure, and has different and species-specific positions on the ventral part of the epitheca. With the vp on the right side of the pore plate, *Az. perforatum* is distinct from *Az. spinosum*, *Az. obesum*, *Az. polongum*, and *Az. asperum* Tillmann (vp on the left side of plate 1'), from *Az. poporum*, *Az. dalianense*, *Az. trinitatum*, *Az. cuneatum* (vp on left side of pore plate), and *Az. caudatum* var. *caudatum* (Halldal) Nézan & Chomérat (vp on right side of plate 1'; see Table 3 in Tillmann *et al.* 2014a). Species that have a vp positioned similarly to *Az. perforatum* (on the cells' right side of the pore plate) are *Az. caudatum* var. *margalefii* (Rampi) Nézan & Chomérat, *Az. concinnum*, *Az. dexteroporum*, *Az. luciferelloides* Tillmann & Akselman, and *Az. zhuanum* Z.Luo, Tillmann & H.Gu (Table 3). These species also have an antapical spine. In *Az. perforatum*, this spine was distinctly tiny, a feature consistent with field specimens (Figs 90–93). Notably, *Az. perforatum* is differentiated from all other *Azadinium* by its unique feature of thecal pores on the pore plate.

Although *Az. perforatum* is larger, it shares some morphological features with *Az. concinnum*, e.g., lack of a stalked pyrenoid, presence of small anterior intercalary plates, and lack of contact between the first precingular

plate and the small first anterior intercalary plate. Otherwise, this feature is found only in *Az. obesum* and *Az. cuneatum* (Tillmann *et al.* 2014a). Moreover, precingular plates of both *Az. perforatum* and *Az. concinnum* are rather large and symmetrically arranged, and both plates 3'' and 4'' are in mid-dorsal position, also seen in species of *Amphidoma* (Dodge & Saunders 1985; Tillmann *et al.* 2012; Tillmann 2018a). It is thus interesting to note that in previous phylogenetic analyses *Az. concinnum* had a rather basal position outside of all other *Azadinium* (Tillmann *et al.* 2019), not unlike the current phylogenetic analysis (Fig. 73). The seemingly large difference in epithelial plate arrangement (*Amphidoma* has six apical plates and no apical intercalary plate, whereas *Azadinium* species have only 3–4 apical plates but 2–3 apical intercalary plates) may also be explained by the fact that there is only one fewer epithelial plate in *Amphidoma*. It is conceivable that the intercalary plates of *Azadinium* are homologous to at least some of the apical plates in *Amphidoma* (Tillmann *et al.* 2014a). In this respect, it is important to note that for *Az. perforatum* a common plate variation was a fusion of apical plates 3' and 2a (Fig. 34), and this deviation was also common among field specimens (Figs 97–99). Next to the number of apical and intercalary plates, another consistent (at least for species of *Amphidoma* studied by SEM) morphological difference between *Azadinium* and *Amphidoma* was recently highlighted (Tillmann 2018a): both differ in



the detailed arrangement of the median sulcal area. For species of *Amphidoma*, the contact between plates Sa and C6 is long and covers almost the whole cingulum width, while for species of *Azadinium* this contact is more narrow, much less than one-third of cingulum width. In this respect, the sulcal area of both *Az. concinnum* and *Az. perforatum* are of the ‘*Azadinium*’ type.

While morphology of *Az. concinnum* and *Az. perforatum*, with their small apical and intercalary plates and the large and symmetrically arranged precingular plates, may indicate a similar and somewhat interim position of both species between *Azadinium* and *Amphidoma*, our phylogenetic analysis shows no close relationship between these species. The new *Az. perforatum* is placed outside of *Azadinium* as a sister clade to *Amphidoma*, whereas *Az. concinnum* is placed at the base within *Azadinium* but only moderately supported. The position of *Az. perforatum* thus indicates higher diversity within Amphidomataceae, potentially also at generic level. However, considering the morphological data and the currently unclear position of *Az. concinnum*, we argue that it is premature to erect a new genus for *Az. perforatum*. In the future, new species/strains of Amphidomataceae and/or new sequences of other marker genes may allow for a more differentiated evaluation of the generic diversity and evolution of the family.

In terms of symmetric precingular plates and relatively small apical and anterior intercalary plates, another similar species was described in 1959 as *Gonyaulax parva* from the Norwegian Sea and Iceland (Ramsfjell 1959). The plate pattern of this species corresponds to the plate tabulation of *Azadinium* and thus should be transferred to *Azadinium* at a later stage. The new species *Az. perforatum* differs from *G. parva* by its different shape (more elongated/slender for *Az. perforatum* than the broader *G. parva*) and by presence of the antapical spine.

The new species *Az. perforatum* is similar in shape to the sketch of a taxon from the Labrador Sea listed by Holmes (1956) as ‘*Goniaulax gracilis* Schiller’. However, this name is just briefly mentioned as ‘uncertain species’ by Schiller (1935) without any description or diagnosis, and is thus not validly described (ICN Art. 38.1). Moreover, the description by Holmes indicates that the Labrador Sea cells are smaller (10–15 µm long) and have a different length:width ratio. In addition, his drawings indicate that the anterior sulcal plate is vaulted and extends close to the apex. Holmes’ observations may thus refer to another undescribed small amphidomatacean species in the area. The name ‘*Goniaulax gracilis*’ sensu Schiller (and thus, likely a member of Amphidomataceae) is also linked to some pictures of small dinophytes in Bérard-Therriault *et al.* (1999; page 216, Fig. 90 a–c, g, i, l). The four LM images probably show species of Amphidomataceae, but no substantiating details are visible. One of the two SEM images (Fig. 90 i) probably represents a species of *Amphidoma* (*Am. languida*?), and the second cell (Fig. 90 l) is probably *Azadinium*, but with a distinct cell outline and a different development and position of the antapical spine than in *Azadinium perforatum*. ‘*Goniaulax gracilis*’ sensu Schiller is also mentioned briefly in a species list (without illustrations) by Smayda (1958) from Jan Mayen (North Atlantic) and by Hsiao (1983) from the Canadian Arctic, which may be

interpreted as evidence that small species of Amphidomataceae are common in cold-water, northern plankton communities.

### Amphidomataceae in Labrador Sea and coastal Greenland waters

Positive hits of the SYBR Green PCR assay indicate that Amphidomataceae are widely distributed in the study area, covering quite different regions including the open, deep Labrador Sea, inland fjord areas such as Godthaab Fjord, Disko Bay and the two northernmost stations. The amphidomatacean SYBR Green PCR assay was not performed quantitatively but relatively high Ct values [cycle threshold (Ct) > 27] indicate a rather low cell abundance for all Greenland stations. Slightly lower Ct values (Ct: 27–30) were observed inside Disko Bay, indicating higher densities than in stations further outside (Ct: 30–33). Generally, low abundance corresponds to a lack of firm identification of amphidomatacean cells during quantitative Utermöhl counts for these stations. A lack of microscopic confirmation does not contradict low PCR signals as the microscopy sample volume was limited (50 ml) and single amphidomatacean cells might easily go unnoticed in the larger group of small unidentified dinoflagellates. Thus, the data underline the advantage of molecular detection at low abundance of this small and inconspicuous group of microalgae.

In the whole Greenland area, only two stations were positive with the species-specific qPCR assays, and both indicate the presence of low background levels of *Azadinium poporum*. This species has a wide distribution in the Mediterranean Sea, the Pacific and the Atlantic (Tillmann 2018b). The northern record reported here needs to be confirmed by more direct methods, as false-positive qPCR reactions cannot be ruled out. Nevertheless, *in silico* sequence comparison of all other known amphidomatacean species with *Az. poporum* primers and probe (Wietkamp, unpublished) identified at least seven base pair mismatch. This underlines the high specificity of the assay, and indicates that risk of a false-positive cross-reaction is low.

The first station in the central Labrador Sea was distinct from the more coastal Greenland stations and had a total plankton biomass approximately three times higher than the Greenland station with the highest biomass (estimated from Utermöhl counts and volume-carbon conversion, unpublished data). In contrast to most coastal Greenlandic stations, diatoms in the central Labrador Sea were of low abundance (absolute and relative) and comprised only 0.6% of total plankton biomass. Plankton at station 1 was dominated by small (< 20 µm) unidentified flagellates ( $1.7 \times 10^6 \text{ l}^{-1}$ ). Most intriguing was the dominance of a *c.* 25 µm large unidentified haptophyte with a short, stiff haptonema and the very unusual presence of *c.* 20 small chloroplasts. Dinoflagellates made up about one-third of the biomass at station 1 with a high density of small athecate species, most of which could not be identified to species level. In contrast to the coastal Greenlandic stations, a significant number of toxigenic cells of *Dinophysis acuminata* ( $330 \text{ l}^{-1}$ ) were present and confirmed the presence of relatively high levels of pectenotoxin-2 (Krock, unpublished). The most abundant phototrophic dinoflagellate was a yet undetermined small



(10–15  $\mu\text{m}$ ) *Prorocentrum* ( $64 \times 10^3$  cells  $\text{l}^{-1}$ ). Within this diverse community, Amphidomataceae were fairly abundant ( $9.2 \times 10^3$  cells  $\text{l}^{-1}$ ) as estimated by quantitative LM, and confirmed by an exceptionally strong signal of the SYBR Green PCR assay ( $\text{Ct } 19.85 \pm 0.06$ ,  $n = 3$ ). The first station in the central Labrador Sea was the only station where the toxigenic species *Am. languida* was recorded by the specific qPCR assay, yielding an abundance of *c.* 120 cells  $\text{l}^{-1}$ , which is in the lower range of cell densities determined for this species along the Danish coast (Wietkamp *et al.* 2019b). In any case, amphidomatacean abundance in the central Labrador Sea in June is lower than bloom concentrations of Amphidomataceae that may be as high as  $10^6$  cells  $\text{l}^{-1}$  (*Az. polongum* bloom in Peru; Tillmann *et al.* 2017) or  $3 \times 10^5$  to  $1 \times 10^7$  cells  $\text{l}^{-1}$  (Amphidomataceae spring bloom densities on Argentine Shelf; Akselman & Negri 2012; Tillmann *et al.* 2019).

Based on both, field-sample-SEM and the amphidomatacean strains established from station 1, a large diversity of Amphidomataceae in the central Labrador Sea is evident. Next to strain-based records of *Az. obesum*, *Az. trinitatum*, *Az. dexteroporum*, and *Az. perforatum*, SEM indicates the presence of *Az. spinosum*, *Am. languida*, and *Az. polongum*. Moreover, another probably yet undescribed species is present whose apical plate number and arrangement conform to *Az. dalianense* (Luo *et al.* 2013), but the position on the ventral pore is different (Figs 107–109). However, no whole-cell views were obtained, and more studies are needed for a more detailed morphological description of this potentially new species.

The ability to establish multiple strains of *Az. obesum*, *Az. trinitatum* and *Az. perforatum* indicates that these are the dominant Amphidomataceae in the summer community of the Labrador Sea. *Azadinium obesum* is known from the North Atlantic Ocean (Tillmann *et al.* 2010, 2018a) and *Az. trinitatum* is known from the Iceland area (Tillmann *et al.* 2014a); thus, their presence in the Labrador Sea was not unexpected.

The new Labrador strains of *Az. trinitatum* form a well-supported sister clade to the Icelandic strains of the species. Uncorrected genetic distance of ITS rDNA between both clades is relatively low (0.006, Table 2), but nevertheless indicates significant intraspecific variability in *Az. trinitatum*. This is supported by the fact that the new strains lack an antapical spine, which is present in Icelandic populations (Tillmann *et al.* 2014a).

The Labrador Sea record of *Az. dexteroporum*, together with a previously established strain from the Irminger Sea (Tillmann *et al.* 2015), confirm the presence of this species in the subarctic region. The new Labrador Sea strain differs significantly from the Mediterranean type material in terms of sequence data (ITS rDNA genetic distance = 0.038, Table 2) and by the presence of a plain median intercalary plate; this plate is distinctly concave in the Mediterranean strain (Percopo *et al.* 2013). All of these facts indicate cryptic diversity for *Az. dexteroporum*, and taxonomic assessment of this diversity should be the objective of future research.

One single cell, most likely representing *Az. spinosum*, was identified in the SEM sample from station 1, but the *Az. spinosum*-specific qPCR assay was negative. This might be explained by abundance below the qPCR detection limit of approx. 0.5 cells  $\text{l}^{-1}$ . Moreover, recent studies have revealed

significant intraspecific variability in *Az. spinosum* in terms of rDNA sequence data (Tillmann *et al.* 2018a, 2019), which likely affects the primer/probe binding efficiency. If *Az. spinosum* in the Labrador Sea is from a different ribotype than that of the *Az. spinosum* strains/ribotype used to design the assay, the assay efficiency and thus detection and quantification of the qPCR method would be affected.

### Azaspiracids

No azaspiracids were detected in discrete plankton samples from the study area. A lack of AZA at the first station, where a cell density of 120 cells  $\text{l}^{-1}$  of the toxigenic *Am. languida* was determined by qPCR, may be explained by the detection limit of the chemical method. Combining the LOD of the AZA measurements ( $10 \text{ pg l}^{-1}$ ) and the highest AZA cell quota of *Am. languida* reported in the literature, of  $100 \text{ fg cell}^{-1}$  (Wietkamp *et al.* 2019b), yields a ‘cell detection limit’ of 100 cells  $\text{l}^{-1}$ , which is only slightly lower than the qPCR-determined abundance. Absence of AZA in field samples also agrees with the lack of AZA production of all newly established strains of *Az. obesum*, *Az. trinitatum*, *Az. dexteroporum* and *Az. perforatum*. For *Az. obesum* and *Az. trinitatum*, this confirms previous study results that neither species are AZA producers (Tillmann *et al.* 2014a; Wietkamp *et al.* 2019b). AZA has unambiguously been described for type strains of *Az. dexteroporum* from the Mediterranean Sea (Rossi *et al.* 2017). However, another strain (1-D12) isolated from the subarctic Irminger Sea lacked AZA (Tillmann *et al.* 2015). Absence of AZA in the new Labrador Sea strains confirms this finding and suggests non-toxicity of *Az. dexteroporum* from the North Atlantic Ocean. A comparable situation with both producing and non-producing strains, with significant levels of sequence differences, can be seen in *Az. poporum* (Luo *et al.* 2018; Wietkamp *et al.* 2019b) and *Az. spinosum* (Tillmann *et al.* 2019). None of the high biomass samples of all three clonal strains of *Az. perforatum* revealed AZA, indicating that this new species likely does not produce AZA. However, with the aforementioned strain variability in *Az. dexteroporum* and the recently discovered intraspecific variability in AZA expression for *Az. poporum* and *Az. spinosum* (Luo *et al.* 2018; Tillmann *et al.* 2019; Wietkamp *et al.* 2019b), more studies and strains of *Az. perforatum* are needed for confirmation. In any case, with 10 non-toxic species versus four known AZA producers, it is evident that AZA production within Amphidomataceae is the exception rather than the rule.

Azaspiracids were also lacking in the SPATT samples from the FerryBox flow-through system. SPATT samplers specifically adsorb large, lipophilic molecules such as AZA (Fux *et al.* 2009; MacKenzie *et al.* 2004), and with long-term deployment (here for about 1 week) allow for integrative sampling to detect minute amounts of these molecules. A lack of AZA detection in SPATT samples thus strengthens the conclusion that abundance and significance of toxigenic Amphidomataceae in June–July for the western Greenland area are low.

### ACKNOWLEDGEMENTS

We thank chief scientist Oliver Zielinski, Captain Maaß and the crew of *RV Maria S. Merian* for assistance and logistical support with the collection of field material used in this study. Anne Müller and

Thomas Max are acknowledged for their help with on-board work during the cruise and especially for DNA and toxin extraction. Torben Krohn (AWI) kindly assisted with AZA sample preparation and analysis. Thanks to Marc Gottschling (Uni München) for helpful discussions.

## FUNDING

This work was supported by the PACES research program of the Alfred Wegener Institute as part of the Helmholtz Foundation initiative in Earth and Environment, and by the German Ministry for Education and Research (project RIPAZA) under grant number 03F0763A.

## ORCID

Haifeng Gu  <http://orcid.org/0000-0002-2350-9171>

## REFERENCES

- Akselman R. & Negri R.M. 2012. Blooms of *Azadinium* cf. *spinosum* Elbrächter et Tillmann (Dinophyceae) in northern shelf waters of Argentina, Southwestern Atlantic. *Harmful Algae* 19: 30–38. DOI: [10.1016/j.hal.2012.05.004](https://doi.org/10.1016/j.hal.2012.05.004).
- Bérard-Therriault L., Poulin M. & Bossé L. 1999. *Guide d'identification du phytoplancton marin de l'estuaire et du golfe de Saint-Laurent incluant également certaines protozoaires. Publication spéciale canadienne des sciences halieutiques et aquatiques* 128. NRC Research Press, Ottawa, Canada. 387 pp.
- Boc A., Diallo A.B. & Makarenkov V. 2012. T-REX: a web server for inferring, validating and visualizing phylogenetic trees and networks. *Nucleic Acids Research* 40: 573–579. DOI: [10.1093/nar/gks485](https://doi.org/10.1093/nar/gks485).
- Brandt K. & Apstein C. [eds] 1908. *Nordisches Plankton*. Lipsius & Tischer, Kiel, Leipzig, Germany. 356pp.
- Cleve P.T. 1873. On diatoms of the Arctic Sea. *Bihang Kongelige Svenska Vetenskapelige Akademi Handlingar* 1(13): 1–28.
- Cleve P.T. & Grunow A. 1880. Beiträge zur Kenntniss der arktischen Diatomeen. *Kongliga Svenska Vetenskaps-Akademiens Handlingar* 17: 1–122.
- Dodge J.D. & Saunders R.D. 1985. An SEM study of *Amphidoma nucula* (Dinophyceae) and description of the thecal plates in *A. caudata*. *Archiv Für Protistenkunde* 129: 89–99. DOI: [10.1016/S0003-9365\(85\)80012-9](https://doi.org/10.1016/S0003-9365(85)80012-9).
- Ehrenberg C.G. 1843. Über neue Anschauungen des kleinsten nördlichen Polarlebens. *Deutsche Akademie Der Wissenschaften Zu Berlin Monatsberichte* 1843: 522–529.
- Elferink S., Neuhaus S., Wohlrab S., Toebe K., Voß D., Gottschling M., Lundholm N., Krock B., Koch B.P., Zielinski O. *et al.* 2017. Molecular diversity patterns among various phytoplankton size-fractions in West Greenland in late summer. *Deep-Sea Research Part I* 121: 54–69. DOI: [10.1016/j.dsr.2016.11.002](https://doi.org/10.1016/j.dsr.2016.11.002).
- Forootan A., Sjöback R., Björkman J., Sjögreen B., Linz L. & Kubista M. 2017. Methods to determine limit of detection and limit of quantification in quantitative real-time PCR (qPCR). *Biomolecular Detection and Quantification* 12: 1–6. DOI: [10.1016/j.bdq.2017.04.001](https://doi.org/10.1016/j.bdq.2017.04.001).
- Fux E., Biré R. & Hess P. 2009. Comparative accumulation and composition of lipophilic marine biotoxins in passive samplers and in mussels (*M. edulis*) on the west coast of Ireland. *Harmful Algae* 8: 523–537. DOI: [10.1016/j.hal.2008.10.007](https://doi.org/10.1016/j.hal.2008.10.007).
- Gran H.H. 1929. Quantitative plankton investigations carried out during the expedition with the “Michael Sars”, July – Sept. 1924. *Rapports Et Procès-verbaux Des Réunions/Conseil Permanent International pour l'Exploration de la Mer* 56: 1–50.
- Grontved J. & Seidenfaden G. 1938. The phytoplankton of the waters west of Greenland. *Meddelelser Om Grønland* 82(5): 1–380.
- Hall T. 1999. BioEdit: a user-friendly biological sequence alignment editor and analysis program for windows 95/98/NT. *Nucleic Acids Symposium Series* 41: 95–98.
- Haldal P. 1953. Phytoplankton investigations from weather Ship M in the Norwegian Sea, 1948–49. *Hvalrådets Skrifter* 38: 1–91.
- Hess P., McCarron P., Krock B., Kilcoyne J. & Miles C.O. 2014. Azaspiracids: chemistry, biosynthesis, metabolism, and detection. In: *Seafood and freshwater toxins*, (Ed. by L.M. Botana), pp. 799–821. CRC Press, Boca Raton, Florida, USA.
- Holmes R.W. 1956. The annual cycle of phytoplankton in the Labrador Sea, 1950–1951. *Bulletin of the Bingham Oceanographic Collection* 16: 1–74.
- Hsiao S.I.C. 1983. A checklist of marine phytoplankton and sea ice microalgae recorded from Arctic Canada. *Nova Hedwigia* 37: 225–313.
- Katoh K. & Standley D.M. 2013. MAFFT multiple sequence alignment software version 7: improvements in performance and usability. *Molecular Biology and Evolution* 30: 772–780. DOI: [10.1093/molbev/mst010](https://doi.org/10.1093/molbev/mst010).
- Keller M.D., Selvin R.C., Claus W. & Guillard R.R.L. 1987. Media for the culture of oceanic ultraphytoplankton. *Journal of Phycology* 23: 633–638. DOI: [10.1111/j.1529-8817.1987.tb04217.x](https://doi.org/10.1111/j.1529-8817.1987.tb04217.x).
- Kilias E., Kattner G., Wolf C., Frickenhaus S. & Metfies K. 2014. A molecular survey of protist diversity through the central Arctic Ocean. *Polar Biology* 37: 1271–1287. DOI: [10.1007/s00300-014-1519-5](https://doi.org/10.1007/s00300-014-1519-5).
- Kilias E., Wolf C., Nöthig E.-M., Peeken I. & Metfies K. 2013. Protist distribution in the western Fram Strait in summer 2010 based on 454-pyrosequencing of 18S rDNA. *Journal of Phycology* 49: 996–1010. DOI: [10.1111/jpy.12109](https://doi.org/10.1111/jpy.12109).
- Lebour M.V. 1925. *The dinoflagellates of the northern seas*. The Marine Biological Association of the United Kingdom, Plymouth, UK. 250 pp.
- Luo Z., Gu H., Krock B. & Tillmann U. 2013. *Azadinium dalianense*, a new dinoflagellate from the Yellow Sea, China. *Phycologia* 52: 625–636. DOI: [10.2216/13-178.1](https://doi.org/10.2216/13-178.1).
- Luo Z., Krock B., Giannakourou A., Venetsanopoulou A., Pagou K., Tillmann U. & Gu H. 2018. Sympatric occurrence of two *Azadinium poporum* ribotypes in the eastern Mediterranean Sea. *Harmful Algae* 78: 75–85. DOI: [10.1016/j.hal.2018.08.003](https://doi.org/10.1016/j.hal.2018.08.003).
- Luo Z., Krock B., Mertens K.N., Nézan E., Chomérat N., Bilien G., Tillmann U. & Gu H. 2017. Adding new pieces to the *Azadinium* (Dinophyceae) diversity and biogeography puzzle: non-toxicogenic *Azadinium zhuanium* sp. nov. from China, toxicogenic *A. poporum* from the Mediterranean, and a non-toxicogenic *A. dalianense* from the French Atlantic. *Harmful Algae* 66: 65–78. DOI: [10.1016/j.hal.2017.05.001](https://doi.org/10.1016/j.hal.2017.05.001).
- MacKenzie L., Beuzenberg V., Holland P., McNabb P. & Selwood A.I. 2004. Solid phase adsorption toxin tracking (SPATT): a new monitoring tool that simulates the biotoxin contamination of filter feeding bivalves. *Toxicon* 44: 901–918. DOI: [10.1016/j.toxicon.2004.08.020](https://doi.org/10.1016/j.toxicon.2004.08.020).
- Medinger R., Nolte V., Pandey R.V., Jost S., Ottenwaelder B., Schloetterer C. & Boenigk J. 2010. Diversity in a hidden world: potential and limitation of next-generation sequencing for surveys of molecular diversity of eucaryotic microorganisms. *Molecular Ecology* 19: 32–40.
- Metfies K., Von Appen W.J., Kilias E., Nicolaus A. & Nöthig E.M. 2012. Biogeography and photosynthetic Biomass of Arctic Marine Pico-Eukaryotes during Summer of the Record Sea Ice Minimum 2012. *PloS One* 11: e0148512.
- Nézan E., Tillmann U., Bilien G., Boulben S., Chèze K., Zentz F., Salas R. & Chomérat N. 2012. Taxonomic revision of the dinoflagellate *Amphidoma caudata*: transfer to the genus *Azadinium* (Dinophyceae) and proposal of two varieties, based on morphological and molecular phylogenetic analyses. *Journal of Phycology* 48: 925–939. DOI: [10.1111/j.1529-8817.2012.01159.x](https://doi.org/10.1111/j.1529-8817.2012.01159.x).
- Nylander J.A., Wilgenbusch J.C., Warren D.L. & Swofford D.L. 2008. AWTY (are we there yet?): a system for graphical exploration of MCMC convergence in Bayesian phylogenetics. *Bioinformatics* 24: 581–583. DOI: [10.1093/bioinformatics/btm388](https://doi.org/10.1093/bioinformatics/btm388).
- Percopo I., Siano R., Rossi R., Soprano V., Sarno D. & Zingone A. 2013. A new potentially toxic *Azadinium* species (Dinophyceae) from the Mediterranean Sea, *A. dexteroporum* sp. nov. *Journal of Phycology* 49: 950–966. DOI: [10.1111/jpy.12104](https://doi.org/10.1111/jpy.12104).
- Posada D. 2008. ModelTest: Phylogenetic model averaging. *Molecular Biology and Evolution* 25: 1253–1256. DOI: [10.1093/molbev/msn083](https://doi.org/10.1093/molbev/msn083).
- Poulin M., Daugbjerg N., Gradinger R., Ilyash L., Ratkova T. & Von Quillfeldt C. 2011. The pan-Arctic biodiversity of marine pelagic and sea-ice unicellular eukaryotes: a first-attempt assessment. *Marine Biodiversity* 41: 13–28. DOI: [10.1007/s12526-010-0058-8](https://doi.org/10.1007/s12526-010-0058-8).

- Preston-Thomas H. 1990. The international temperature scale of 1990 (ITS-90). *Metrologia* 27: 3–10. DOI: [10.1088/0026-1394/27/1/002](https://doi.org/10.1088/0026-1394/27/1/002).
- Ramsfjell E. 1959. Two new phytoplankton species from the Norwegian Sea, the diatom *Coscinosira poroseriata*, and the dinoflagellate. *Gonyaulax Parva*. *Nytt Magazin for Botanikk* 7: 175–177.
- Ronquist F. & Huelsenbeck J.P. 2003. MrBayes 3: Bayesian phylogenetic inference under mixed models. *Bioinformatics* 19: 1572–1574. DOI: [10.1093/bioinformatics/btg180](https://doi.org/10.1093/bioinformatics/btg180).
- Rossi R., Dell'Aversano C., Krock B., Ciminiello P., Percopo I., Tillmann U., Soprano V. & Zingone A. 2017. Mediterranean *Azadinium dexteroporum* (Dinophyceae) produces AZA-35 and six novel azaspiracids: a structural study by a multi-platform mass spectrometry approach. *Analytical and Bioanalytical Chemistry* 409: 1121–1134. DOI: [10.1007/s00216-016-0037-4](https://doi.org/10.1007/s00216-016-0037-4).
- Schiller J. 1935. Dinoflagellatae (Peridineae) in monographischer Behandlung. In: *Dr. L. Rabenhorst's Kryptogamen-Flora von Deutschland, Österreich und der Schweiz*, (Ed. by L. Rabenhorst), pp. 1–320. Akademische Verlagsgesellschaft, Leipzig, Germany.
- Schlitzer R. 2018. Ocean data view. <https://odv.awi.de>.
- Smayda T.J. 1958. Phytoplankton studies around Jan Mayen Island March - April, 1955. *Nytt Magazin for Botanikk* 6: 75–96.
- Smith K.F., Rhodes L., Harwood D.T., Adamson J., Moisan C., Munday R. & Tillmann U. 2016. Detection of *Azadinium poporum* in New Zealand: The use of molecular tools to assist with species isolations. *Journal of Applied Phycology* 28: 1125–1132. DOI: [10.1007/s10811-015-0667-5](https://doi.org/10.1007/s10811-015-0667-5).
- Stamatakis A. 2006. RAxML-VI-HPC: Maximum likelihood-based phylogenetic analyses with thousands of taxa and mixed models. *Bioinformatics* 22: 2688–2690. DOI: [10.1093/bioinformatics/btl446](https://doi.org/10.1093/bioinformatics/btl446).
- Swofford D.L. 2002. *PAUP\*: phylogenetic analysis using parsimony (\* and other methods)*, version 4.0b10. Sinauer Associates, Sunderland, Massachusetts, USA.
- Thronsen J., Hasle G.R. & Tangen K. 2007. *Phytoplankton of Norwegian coastal waters*. Almatier Forlag AS, Oslo, Norway. 343 pp.
- Tillmann U. 2018a. Electron microscopy of a 1991 spring plankton sample from the Argentinean shelf reveals the presence of four new species of Amphidomataceae (Dinophyceae). *Phycological Research* 66: 269–290. DOI: [10.1111/pre.12225](https://doi.org/10.1111/pre.12225).
- Tillmann U. 2018b. Amphidomataceae. In: *Harmful Algae Blooms, a compendium desk reference*, (Ed. by S.E. Shumway, J.A. Burkholder & S.L. Morton), pp. 575–582. Wiley, Hoboken, New Jersey, USA.
- Tillmann U. & Akselman R. 2016. Revisiting the 1991 algal bloom in shelf waters off Argentina: *Azadinium luciferelloides* sp. nov. (Amphidomataceae, Dinophyceae) as the causative species in a diverse community of other amphidomataceans. *Phycological Research* 64: 160–175. DOI: [10.1111/pre.2016.64.issue-3](https://doi.org/10.1111/pre.2016.64.issue-3).
- Tillmann U., Edvardsen B., Krock B., Smith K.F., Paterson R.F. & Voß D. 2018a. Diversity, distribution, and azaspiracids of Amphidomataceae (Dinophyceae) along the Norwegian coast. *Harmful Algae* 80: 15–34. DOI: [10.1016/j.hal.2018.08.011](https://doi.org/10.1016/j.hal.2018.08.011).
- Tillmann U., Elbrächter M., John U., Krock B. & Cembella A. 2010. *Azadinium obesum* (Dinophyceae), a new nontoxic species in the genus that can produce azaspiracid toxins. *Phycologia* 49: 169–182. DOI: [10.2216/PH09-35.1](https://doi.org/10.2216/PH09-35.1).
- Tillmann U., Elbrächter M., Krock B., John U. & Cembella A. 2009. *Azadinium spinosum* gen. et sp. nov. (Dinophyceae) identified as a primary producer of azaspiracid toxins. *European Journal of Phycology* 44: 63–79. DOI: [10.1080/09670260802578534](https://doi.org/10.1080/09670260802578534).
- Tillmann U., Gottschling M., Guinder V. & Krock B. 2018b. *Amphidoma parvula* (Amphidomataceae), a new planktonic dinophyte from the Argentine Sea. *European Journal of Phycology* 53: 14–28. DOI: [10.1080/09670262.2017.1346205](https://doi.org/10.1080/09670262.2017.1346205).
- Tillmann U., Gottschling M., Krock B., Smith K.F. & Guinder V. 2019. High abundance of Amphidomataceae (Dinophyceae) during the 2015 spring bloom of the Argentinean Shelf and a new, non-toxicogenic ribotype of *Azadinium spinosum*. *Harmful Algae* 84: 244–260. DOI: [10.1016/j.hal.2019.01.008](https://doi.org/10.1016/j.hal.2019.01.008).
- Tillmann U., Gottschling M., Nézan E. & Krock B. 2015. First record of *Azadinium dexteroporum* and *Amphidoma languida* (Amphidomataceae, Dinophyceae) from the Irminger Sea off Iceland. *Marine Biodiversity Records* 8: 1–11. DOI: [10.1017/S1755267215001128](https://doi.org/10.1017/S1755267215001128).
- Tillmann U., Gottschling M., Nézan E., Krock B. & Bilien G. 2014a. Morphological and molecular characterization of three new *Azadinium* species (Amphidomataceae, Dinophyceae) from the Irminger Sea. *Protist* 165: 417–444. DOI: [10.1016/j.protis.2014.04.004](https://doi.org/10.1016/j.protis.2014.04.004).
- Tillmann U., Krock B. & Taylor B. 2014b. *Azadinium caudatum* var. *margalefii*, a poorly known member of the toxicogenic genus *Azadinium* (Dinophyceae). *Marine Biology Research* 10: 941–956. DOI: [10.1080/17451000.2013.866252](https://doi.org/10.1080/17451000.2013.866252).
- Tillmann U., Salas R., Gottschling M., Krock B., O'Driscoll D. & Elbrächter M. 2012. *Amphidoma languida* sp. nov. (Dinophyceae) reveals a close relationship between *Amphidoma* and *Azadinium*. *Protist* 163: 701–719. DOI: [10.1016/j.protis.2011.10.005](https://doi.org/10.1016/j.protis.2011.10.005).
- Tillmann U., Sánchez-Ramírez S., Krock B. & Bernal-Jiménez A. 2017. A bloom of *Azadinium polongum* in coastal waters off Peru. *Revista De Biología Marina Y Oceanografía* 52: 591–610. DOI: [10.4067/S0718-19572017000300015](https://doi.org/10.4067/S0718-19572017000300015).
- Toebe K., Joshi A.R., Messtorff P., Tillmann U., Cembella A. & John U. 2013. Molecular discrimination of taxa within the dinoflagellate genus *Azadinium*, the source of azaspiracid toxins. *Journal of Plankton Research* 35: 225–230. DOI: [10.1093/plankt/fbs077](https://doi.org/10.1093/plankt/fbs077).
- Twiner M., Hess P. & Doucette G.J. 2014. Azaspiracids: toxicology, pharmacology, and risk assessment. In: *Seafood and freshwater toxins*, (Ed. by L.M. Botana), pp. 823–855. CRC Press, Boca Raton, Florida, USA.
- Wassmann P., Duarte C.M., Agustí S. & Sejr M.K. 2011. Footprints of climate change in the Arctic marine ecosystem. *Global Change Biology* 17: 1235–1249. DOI: [10.1111/gcb.2010.17.issue-2](https://doi.org/10.1111/gcb.2010.17.issue-2).
- Wietkamp S., Krock B., Gu H., Voß D., Klemm K. & Tillmann U. 2019b. Occurrence and distribution of Amphidomataceae (Dinophyceae) in Danish coastal waters of the North Sea, the Limfjord, and the Kattegat/Belt area. *Harmful Algae* 88: 101637. DOI: [10.1016/j.hal.2019.101637](https://doi.org/10.1016/j.hal.2019.101637).
- Wietkamp S., Tillmann U., Clarke D. & Toebe K. 2019a. Molecular determination and quantification of the toxicogenic dinoflagellate *Amphidoma languida* (Amphidomataceae, Dinophyceae). *Journal of Plankton Research* 41: 101–113. DOI: [10.1093/plankt/fby052](https://doi.org/10.1093/plankt/fby052).
- Wolf C., Kiliyas E. & Metfies K. 2015. Protists in the polar regions: comparing occurrence in the Arctic and Southern Oceans using pyrosequencing. *Polar Research* 34: 23225. DOI: [10.3402/polar.v34.23225](https://doi.org/10.3402/polar.v34.23225).
- Xiao X., Sogge H., Lagesen K., Tooming-Klunderud A., Jakobsen K.S. & Rohrlack T. 2014. Use of high throughput sequencing and light microscopy show contrasting results in a study of phytoplankton occurrence in a freshwater environment. *PloS One* 9: e106510. DOI: [10.1371/journal.pone.0106510](https://doi.org/10.1371/journal.pone.0106510).
- Zielinski O., Braun A., Henkel R., Mascarenhas V.J., Meier D. & Voß D. 2018. *Physical oceanography during Maria S. Merian cruise MSM65 (GREENHAB II)*. Institute for Chemistry and Biology of the Marine Environment, Carl-von-Ossietzky University of Oldenburg, Germany. PANGAEA. DOI: [10.1594/PANGAEA.886181](https://doi.org/10.1594/PANGAEA.886181).